

PRODUCTION OF NO_x IN AN ALTERNATING
CURRENT PLASMA REACTOR

By

SCOTT B. ROBINOWITZ

Bachelor of Engineering

Tulane University

New Orleans, Louisiana


1991

Submitted to the Faculty of the
Graduate College of the
Oklahoma State University
in partial fulfillment of
the requirements for
the Degree of
MASTER OF SCIENCE
December, 1992

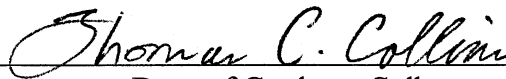
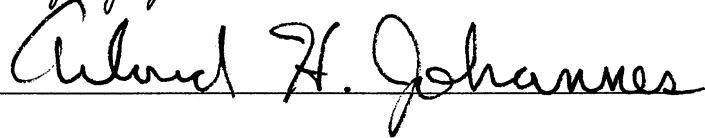
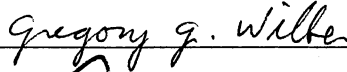
Thesis
1992
R656p

PRODUCTION OF NO_x IN AN ALTERNATING
CURRENT PLASMA REACTOR

Thesis Approved:



Thesis Adviser



Dean of Graduate College

TABLE OF CONTENTS

Chapter	Page
I. INTRODUCTION	1
II. LITERATURE REVIEW	6
Controlled Ecological Life Support Systems	6
Gas Breakdown and Breakdown Voltage	9
Corona Chemistry	12
Toxic Byproducts From the Reactor	13
Nitrogen Oxide Chemistry	16
Destruction Feasibility	18
III. EXPERIMENTAL APPARATUS, PROCEDURE AND ANALYSIS	25
Reactor Geometry and Dimensions	25
Discharge System	26
Experimental Apparatus	28
Experimental Procedure and Analysis	32
Reactor Optimization	32
Experimental Design	39
Additional Testing	40
Primary Voltage Variation	41
Frequency Variation	42
Flow Rate Variation	42
Relative Humidity Variation	43
Chemical Reaction and Mechanism Validation	44
IV. REACTOR OPTIMIZATION	45
Results and Discussion	45
Power Dependence on Frequency and Primary Voltage	45
Plasma Behavior with Respect to Humidity	47

Chapter	Page
V. NO _x PRODUCTION TESTS	50
Preliminary Testing Realizations	50
Dependence of NO _x Production on Primary Voltage	52
Dependence of NO _x Production on Frequency	52
Dependence of NO _x Production on Flow Rate	55
Dependence of NO _x Production on Relative Humidity	55
Possible Reasons for NO _x Increase	58
Possible Reasons for NO _x Decrease	60
Brief Note on Plasma Stability	61
VI. ADDITIONAL TESTING	63
Destruction Testing	63
Validation of Chemical Reaction Mechanisms	63
VII. CONCLUSIONS AND RECOMMENDATIONS	69
Conclusions	69
Recommendations	70
BIBLIOGRAPHY	71
APPENDIX A - SAMPLE CALCULATIONS	75
APPENDIX B - REACTOR OPTIMIZATION TEST DATA	77
APPENDIX C - NO _x PRODUCTION TEST DATA	82
APPENDIX D - NO _x DESTRUCTION TEST DATA	86
APPENDIX E - ION CHROMATOGRAPH COLUMN RESPONSE	88
APPENDIX F - NITRITE AND NITRATE CONCENTRATIONS DEDUCED FROM ION CHROMATOGRAPH TESTING	90

LIST OF TABLES

Table	Page
1. Consumables Required to Support a 70 Kg human Being for One Year	8
2. Corona Starting Gradient for Various Gases	11
3. Decomposition Efficiencies of DMMP and TMP in an ACPR	22
4. Decomposition Efficiency of PFA in an ACPR	23
5. Destruction of HCN in an ACPR	23
6. Other Destruction Feasibility Studies	24
7. Reactor Optimization Test Data Corresponding to Figure 14 Run 1	78
8. Reactor Optimization Test Data Corresponding to Figure 14 Run 2.	78
9. Reactor Optimization Test Data Corresponding to Figure 14 Run 3	79
10. Reactor Optimization Test Data Corresponding to Figure 14 Run 4.	80
11. Reactor Optimization Test Data Corresponding to Figures 14 & 15 Run 5.	80
12. Reactor Optimization Test Data Corresponding to Figure 16 Run 6.	81
13. NO _x Production vs Primary Voltage Test Data Corresponding to Figure 17, Runs 7, 8, & 9	83

Table		Page
14.	NOx Production vs Frequency Test Data Corresponding to Figure 18, Runs 10 & 11	83
15.	NOx Production vs Flow Rate Test Data Corresponding to Figure 19, Runs 12, 13, & 14	84
16.	NOx Production vs Relative Humidity Test Data Corresponding to Figure 20, Runs 15 & 16	84
17.	NOx Destruction vs Flow Rate Test Data Corresponding to Figure 22, Run 17	87
18.	NOx Destruction vs Flow Rate Test Data Corresponding to Figure 22, Run 18	87
19.	Concentration Data From Various Samples Using the Ion Chromatograph Corresponding to Figures 23,.24 & 25	91

LIST OF FIGURES

Figure	Page
1. Alternating Current Plasma Reactor (ACPR)	4
2. Level of Recycling Necessary to Make Space Missions Economically Feasible with Respect to Mission Duration. Numbered Intersections Correspond to Duration that the Indicated Level of Recycling is Economically Necessary	8
3. Mechanism for Corona Creation	14
4. Illustration of Corona Generation's Dependence on Frequency	15
5. Alternating Current Plasma Reactor (ACPR) Annular Volume = 74.78 cm ³	27
6. Schematic of Experimental Apparatus	29
7. Cold Trap Condensing Chamber	31
8. Breathing Air Streams 1 & 2, Flow Control Modules and Gas Dryer	33
9. Humidity Source and Junction for Streams One and Two	34
10. Humidity Probe and Monitoring Port	35
11. Alternating Current Plasma Reactor and Apparatus Under the Hood	36
12. Discharge System and Electrical Monitoring Apparatus	37
13. Chemiluminescent NO _x Analyzer	38

Figure	Page
14. Dependence of Reactor Power Input on Frequency for Air at Fixed Primary Voltages and 118 ml/min	46
15. Relationship of Power and Secondary Voltage to Frequency at a Primary Voltage of 60 and 118 ml/min	48
16. Effect of Humidity on Plasma Behavior	49
17. NO _x Production with Respect to Primary Voltage Dry Air @ 118 ml/min	53
18. NO _x Production with Respect to Frequency at 60 volts. Dry Air @ 118 ml/min	54
19. NO _x Production with Respect to Flow Rate at 60 volts. Dry Air	56
20. NO _x Production with Respect to Relative Humidity at 60 volts Flow Rate 146 ml/min	57
21. Representation of Possible NO _x Production Mechanisms with Respect to Relative Humidity	62
22. NO _x Destruction with Respect to Flow Rate using a 7459 ppm Nitric Oxide, NO, Standard @ Optimized 60 volt Setting	64
23. Graphical Representation of Nitrate Concentration in Condensate 1:100,000 Dilution Nitrate Peak Occurs at 3.48 and has a Value of 137718, Indicated by the Dionex Ion Chromatograph	66
24. Graphical Representation of Nitrite & Nitrate Concentrations in the NaOH Solution. 1:100 Dilution Nitrite Peak Occurs at 1.93 and has a Value of 55111, Nitrate Peak Occurs at 3.56 and has a Value of 16385 as Indicated by the Dionex Ion Chromatograph	67

CHAPTER I

INTRODUCTION

Space travel is now entering a new frontier. Short term missions are no longer the forefront of space technology. The next era of space travel could possibly be 5-year deep space explorations, or space colony cultivation. A primary concern when considering lengthy space travel is life support. Presently, all supplies needed to sustain life are brought from earth to satisfy human needs for the duration of the mission. The cost for transporting a gallon of water to the moon is about half a million dollars (10). At that price, 1 year of consumable necessities (food, oxygen, etc.) loaded aboard would make a mission uneconomical. It becomes obvious that a recycling life support system is a must. A bioregenerative system is the life support system of the not-so-distant future.

In a bioengineered environment, i.e. a space station life support system, atmospheric conditions similar to earth, ideally, would be reproduced as closely as possible to provide a safe, predictable, and productive artificial environment. Currently, spacecraft life support systems rely on open-loop (non recycling) technologies. These systems are sufficiently reliable for human space-flight missions of relatively short duration, small crew size and limited power availability. Life support technologies for the coming era of exploration, however, must address a different set of requirements. Longer duration missions, larger crew sizes, and crew variation during the mission, will require an increased degree of self-sufficiency of the life-support system to enhance crew safety. This self-sustaining system will minimize

the economic costs associated with resupply and the accompanying complexity of logistics, while maintaining a familiar, earth like living environment to promote human productivity and psychological well-being (9).

Ongoing research at the John F. Kennedy Space Center is currently demonstrating the feasibility of utilizing a higher plant based engineering paradigm for advanced life support in a Controlled Ecological Life Support System (CELSS). Such a higher plant based system would ideally utilize the plants for a direct food source, for gas exchange, water reclamation, and the plant residuals in a complex biological resource recovery scheme (8).

The natural interaction between plants and humans provides the theoretical basis for the CELSS. Gas exchange is achieved by the reciprocating relationship between plants and humans. Humans exhale carbon dioxide and plants, through photosynthesis, produce oxygen. Wastes from one section of the bioregenerative system, is another section's necessary nutrients to continue its tasks. In closed life support systems, the balance is delicate, complex, and entirely dependent on such environmental conditions as temperature, pressure, and light, as well as the biological processes of the community of microorganisms, their interaction with one another, and the plant community.

The compounds of nitrogen are of great interest to environmental engineers because of the importance of nitrogen compounds in the atmosphere and in the life processes of all plants and animals (37). For proper plant growth to proceed, various macro- and micro-nutrients must be present in the growing medium. One of the many problems being addressed in the design of the CELSS is plant growth in an artificial environment. In this controlled environment, a foreseen shortage of nitrates will exist (8). The main source of NO_x in the earth's lower atmosphere is emission of NO at the earth's surface, either from soil processes or from man made combustion sources. Also, lightning, a concentrated electric discharge, oxidizes atmospheric nitrogen, N₂,

to form nitrogen oxides. These oxides then react with water vapor and are deposited on the earth as nitric acid (18). This natural nitric acid deposition provides plant life with nitrate, a necessary macro-nutrient. As mentioned above, lightning oxidizes nitrogen, which is eventually deposited as nitric acid and broken down by the soil and plants to nitrates. In a space station, there will be no lightning, thus, the lack of natural oxidation of N_2 will result in a nitrate shortage, impeding proper plant activity. The CELSS will grow plants hydroponically, i.e. without soil, no combustion sources will be present and, as mentioned above, lightning will not exist. These operating conditions detail the foreseen shortage of nitrates which are necessary for life support system balance (8). Soil would add unnecessary weight to the spacecraft leaving Earth driving the mission toward economic impossibility. The above restrictions that the CELSS operate under yield a nitrate shortage that must be remedied.

When a nitrate shortage is experienced on earth, how is the problem handled? People spread fertilizer on their lawns. A bag of fertilizer is practically all nitrates. Why doesn't NASA bring bags of fertilizer to remedy the foreseen nitrate shortage? Again, cost per pound to lift items into space very quickly becomes prohibitive. A 20 lb bag of fertilizer would cost upwards of 2 million dollars to launch into space (10). An efficient, lightweight method to produce the oxides of nitrogen is needed to bring the bioregenerative life support system one step closer to reality.

The overall objective of the work is to investigate the feasibility of using an alternating current plasma reactor (ACPR) to produce oxides of nitrogen. The reactor used in this work was developed as a joint venture by the Naval Research Center and Oklahoma State University.

A plasma reactor utilizes electrical energy to create a low temperature plasma (electric discharge) in a reactor cavity (see Figure 1). When reactants flow into the

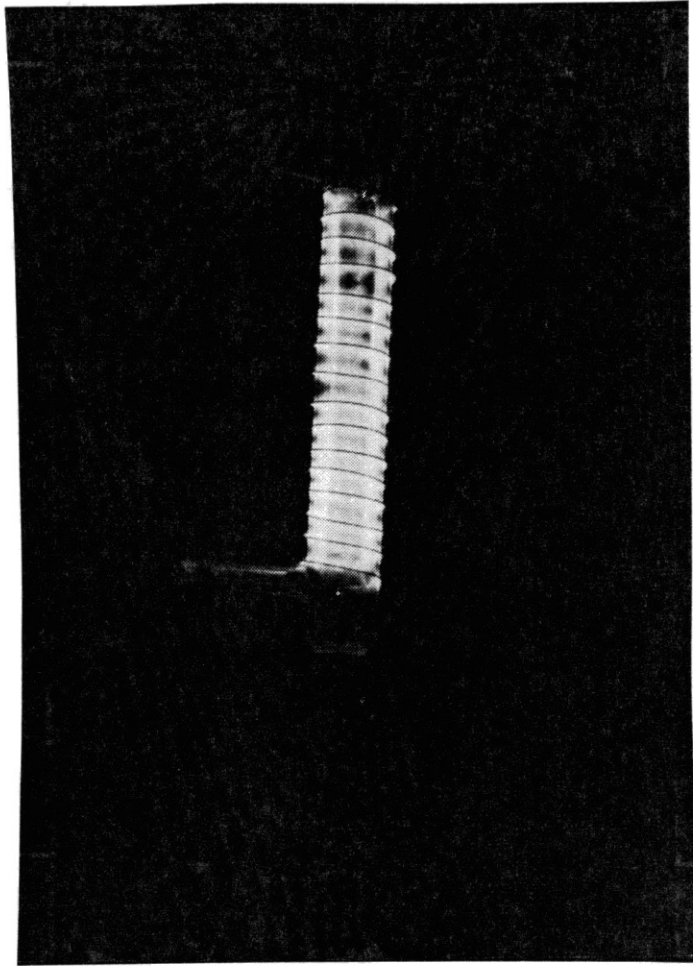


Figure 1. Alternating Current Plasma Reator (ACPR)

discharge chamber, their chemical bonds are broken by absorbing the electrical energy of the plasma. Elemental atoms result, which then recombine to form the reaction byproducts.

To date, the ACPR has predominantly been studied as a method to remove toxic contaminants from air streams. Much work needs to be done understanding the relationships between plasma variables (power, frequency, gas type) and byproduct formation. The predominant toxic byproducts formed with an air carrier in an ACPR are ozone, carbon monoxide and NO_x (1). Ozone has been investigated thoroughly in efforts to develop an efficient ozone generator to be used in various water purification systems. Tevault et al. (3) briefly investigated NO_x production in a silent discharge reactor as a function of frequency, power, and humidity.

This research will attempt to prove the ACPR is an efficient method to generate the oxides of nitrogen at approximate atmospheric conditions. Tanked breathing air will be used as the reactant gas stream. This will closely mimic the foreseen CELSS atmosphere.

The specific objectives of this research are:

1. To conduct NO_x production testing and to develop an understanding of how production varies with respect to input electrical plasma characteristics (i.e. primary voltage and frequency).
2. To conduct NO_x production testing exploring the relationship between production and assorted reactant gas flow variables (i.e. flow rate and humidity).
3. To use information gathered from above objectives to maximize NO_x production from the ACPR.
4. To perform a preliminary study in order to confirm the plasma chamber as a feasible method for NO_x destruction.

CHAPTER II

LITERATURE REVIEW

Plasma and plasma mechanics have been studied extensively for the past 80 years. Researchers have investigated various power sources, plasma chamber geometries, and destruction feasibility for many airborne pollutants. Alternatively, the CELSS technology is a relatively new field of study, but recently much work has been done attempting to fully understand how to control an engineered system with so many interrelated variables. Due to the volume and diversity of works presented in the literature much of the background work on plasmas is beyond the scope of this review. Instead, the following literature survey covers the background of controlled ecological life support systems, (CELSS), as well as gas breakdown and breakdown voltage. The basis of plasma chemistry and nitrogen oxide chemistry will be explained. To provide validity for the pilot NO_x destruction testing, adverse health and environmental effects of nitrous oxides will be covered as well as a short investigation of past destruction studies carried out utilizing the ACPR.

Controlled Ecological Life Support Systems

As we approach the twenty-first century, the United States moves closer to a new era in space exploration. This new era promises interplanetary transportation and the establishment of outposts on other planets. Success in this exploration depends on many different technologies: some already mature, some

currently under development, and others still in the conceptual stages. Particularly crucial are the technologies that support human life (9). A human requires substantial amounts of consumable materials to sustain life. Table 1 illustrates the estimates required for a 70 kg person to live for one year. Consequently, supplying all these consumables from Earth is an extremely expensive proposition. As a result, the development of technologies that recycle wastes and regenerate consumables is both logistically and economically essential. Myers developed a method of determining break-even points for missions employing various degrees of recycling, shown in Figure 2 (9). Full recycling would pay off only on long missions, but, as can be seen, water recycling and atmosphere regeneration would be worthwhile on shorter missions. Since we are considering missions of five years or longer, a fully recycling system is an economic necessity.

A controlled ecological life support system (CELSS) is an engineered system that controls and balances the metabolic byproducts of plants and animals to provide life support in a closed system such as a spacecraft, seafloor, or extraterrestrial colony. Future space and seafloor colonies, long-term space missions, and manned stellar voyages will undoubtedly rely primarily on CELSS simply because enough consumables cannot possibly be carried along for years of life support (11). In the CELSS approach envisioned by NASA, a specifically designed and tightly managed environment is strictly engineered for the higher plants which will promote maximal crop production and allow enough flexibility for various manipulations of the crop output (10). Research of the last decade has shown that all human life support needs can be met by a bioregenerative life support system based on higher plants, algae, or a combination of both (9). Through photosynthesis, plants convert carbon dioxide and water to carbohydrates and oxygen: through transpiration, they produce potable water; and, by their use of inorganic elements, they are in a position to reclaim many components of human and plant wastes.

TABLE 1
 CONSUMABLES REQUIRED TO SUPPORT A 70 KG
 HUMAN BEING FOR ONE YEAR

Consumable Item	Mass (kg/year)
Food (dry mass)	219
Oxygen	329
Drinking water	657
Sanitary water	840
Domestic water	6132

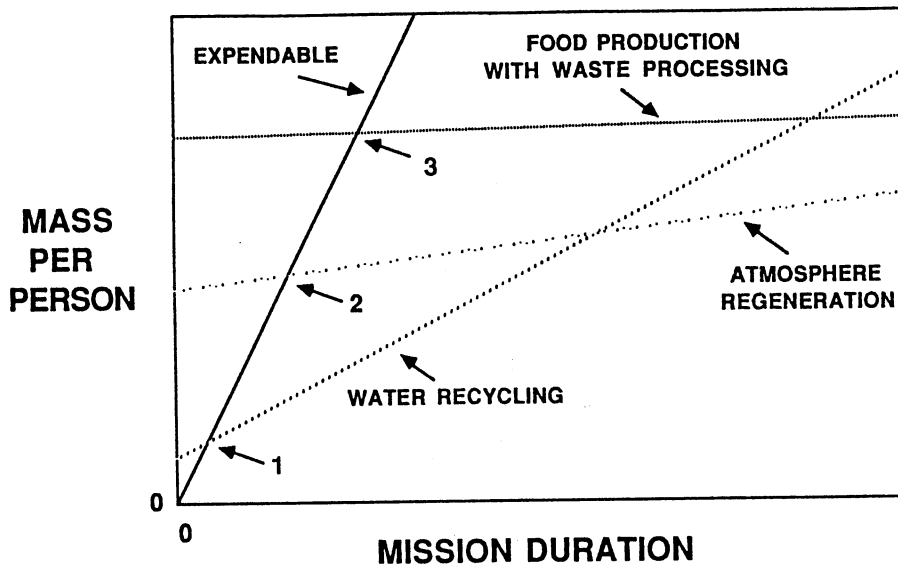


Figure 2. Level of Recycling Necessary to Make Space Missions
 Economical Feasible with Respect to Mission Duration.
 Numbered Intersections Correspond to Duration
 that the Indicated Level of Recycling
 is Economically Necessary

Strictly speaking, there are no wastes in a CELSS, only resources. Again, for the bioregenerative system to support life, all necessary nutrients must be present for all species to survive and carry out their specific tasks. If plant life has no source of nitrates, the process of photosynthesis will be impeded, and eventually cease. This will lead to a breakdown in the delicate life support system, causing all life forms to die.

Gas Breakdown and Breakdown Voltage

A gas has a very low electrical conductivity, resulting from a relatively small number of free electrons and positive and negative ions. However, when an electric field is applied, electrons gain more energy than the ionization energy of the gas molecules. At this time, the molecule is capable of ionizing. This new electron, together with the primary one, repeats the process and produces an avalanche of electrons. Such generation of rapidly succeeding avalanches can produce a space charge of slow positive ions in the gap which favors the ionization conditions for the electrons, and produces the rapid current growth leading to "breakdown" (12). A manifestation of discharge or breakdown is emission of light, sometimes accompanied by audible noise and by current fluctuations (23).

Liao and Plumb (5) concluded that the breakdown of air in a non-uniform field was always at a lower voltage than in a uniform field. For moderately non-uniform field electrodes such as coaxial cylinders, the breakdown voltages increased linearly, with increased electrode spacing as in a uniform field. As the spacing between electrodes became comparable to, or greater than the diameter of either electrode, the breakdown value increased more slowly with increasing spacing. For very non-uniform field electrodes, such as a wire electrode, the breakdown characteristics were not so regular.

Liao and Plump (5) also found that the irregular breakdown of very non-uniform fields was attributed to space charges produced by local ionization prior to breakdown in

the gap. For some gases, such as nitrogen, only positive-ion space charges could be produced. For air, negative-ion space charges due to oxygen were also present which, even in a relatively small quantity, tended to complicate the breakdown in an air gap. However, for electronegative gases, which could produce a large amount of negative-ion space charges upon ionization, the breakdown characteristics were found to be very irregular.

Thorton (24) measured the corona-starting gradients in wire-cylinder gaps. He used a 50 Hz alternating voltage in his experiments. The gradients are shown in Table 2 for a number of gases at 760 mm Hg and 0 degrees C.

For concentric cylindrical electrodes with two dielectric layers, the total voltage, $V(b)$, necessary to initiate the corona in the gas gap could be evaluated by the following equation (39).

$$V_b = 0.5 E D_2 K_g \delta \left(\frac{\ln(D_2/D_1)}{K_d} + \frac{\ln(D_3/D_2)}{K_g} + \frac{\ln(D_4/D_3)}{K_d} \right) \quad (2.1)$$

This equation can be used to calculate the starting gradient in any gas.

- where
- K_d = dielectric constant of barrier
 - K_g = dielectric constant of gas
 - D_1 = inner diameter of the inner tube, cm
 - D_2 = outer diameter of the inner tube, cm
 - D_3 = inner diameter of the outer tube, cm
 - D_4 = outer diameter of the outer tube, cm

Table 2

CORONA STARTING GRADIENT FOR VARIOUS GASES

Gas	Corona Starting Gradient Voltage (Kv/cm)
Air	35.5
H ₂	15.5
He	4.0
O ₂	29.1
N ₂	38.0
Cl ₂	85.0
CO	45.5
CO ₂	26.2
NH ₃	56.7
N ₂ O	55.3
H ₂ S	52.1
SO ₂	67.2
CS ₂	64.2
CH ₄	22.3
CH ₂ Cl ₂	126.0
CHCl ₃	162.0
CCl ₄	204.0
CH ₃ Cl	45.6
CH ₃ I	75.0
CH ₃ Br	97.0

Corona Chemistry

The idea of utilizing corona discharges for chemical catalysis goes back 100 years. Early experimenters with high-voltage electricity learned how to establish a corona in a chemical reactor, preventing the development of an arc by placing a glass or other insulating barrier in the path of the gas breakdown. The interaction of high-voltage electricity with matter seemed baffling, there were widely fluctuating yields and electrical equipment was undependable. The only commercially significant development of the early corona work was the process for making ozone, O₃, by subjecting oxygen to corona in an "ozonizer" (1). To achieve an efficient process, whether it be the destruction of gaseous contaminants or the production of gaseous byproducts, the plasma must attain stability. Stability occurs when ample time has passed to allow all internal plasma variables to reach a steady state.

After World War II, advances in technology made corona chemistry a more promising field. High frequency power could be generated at a reasonable cost. Improved electronic components and circuitry made it easier to tune, control and measure corona power (1).

Knowledge of radiation chemistry is relevant to corona research because both areas deal with "free radicals" formed by electron impact. A radical is a molecular fragment that functions as a unit. Ordinarily, radicals are linked to other atoms by covalent bonds to form molecules. When a bond is broken, the radical is left with one or more unshared electrons. In this condition, the radical is ready to combine with another atom or group of atoms; it is so extremely reactive that it usually exists as a free radical for a fraction of a second at most (1).

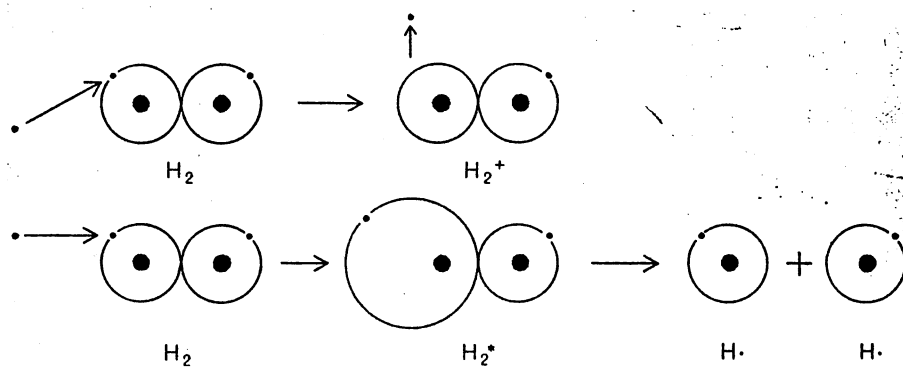
The phenomenon of corona starts with the few stray electrons that are always present in a gas due to cosmic rays or other background radiation. If a high voltage (10,000 - 15,000 volts) is applied, creating a strong electric field, the electrons are

accelerated toward the positive electrode. The electrons strike gas molecules in their path, from which they rebound with little loss of energy because of the great disparity in mass -- like a ping pong ball rebounding from a bowling ball. Then the process repeats itself. Occasionally, a long enough path opens up for an electron, so that when it finally hits a gas molecule it has acquired enough energy to penetrate the molecule's shield or orbiting electrons. The impacting electron may knock an orbital electron out of the molecule, leaving a positive ion and another free electron that can go on to strike another molecule. Or, as is more often the case, the impacting electron lifts an orbiting electron to an unstable, higher energy orbit, creating an "excited" molecule. Soon the gas is full of electrons, positive ions, excited molecules, heat and light -- or in other words, corona. The excited molecules are unstable, and decompose spontaneously into free radicals. The whole process of corona buildup takes only about one ten-millionth of a second, and it is repeated every time the electric field reverses (1).

The importance of frequency stems from the mechanism of corona formation explained above (see Figures 3 and 4). The burst of corona activity begins as the voltage rises on each half-cycle. As the electrons and positive ions become concentrated at the opposite electrodes, they build up a space charge that neutralizes the electric field and chokes the corona. When the field is reversed, the space charge is dissipated and another corona burst can occur. The number of bursts, the current draw, and the rate of chemical reaction are, therefore, approximately proportional to the frequency (1).

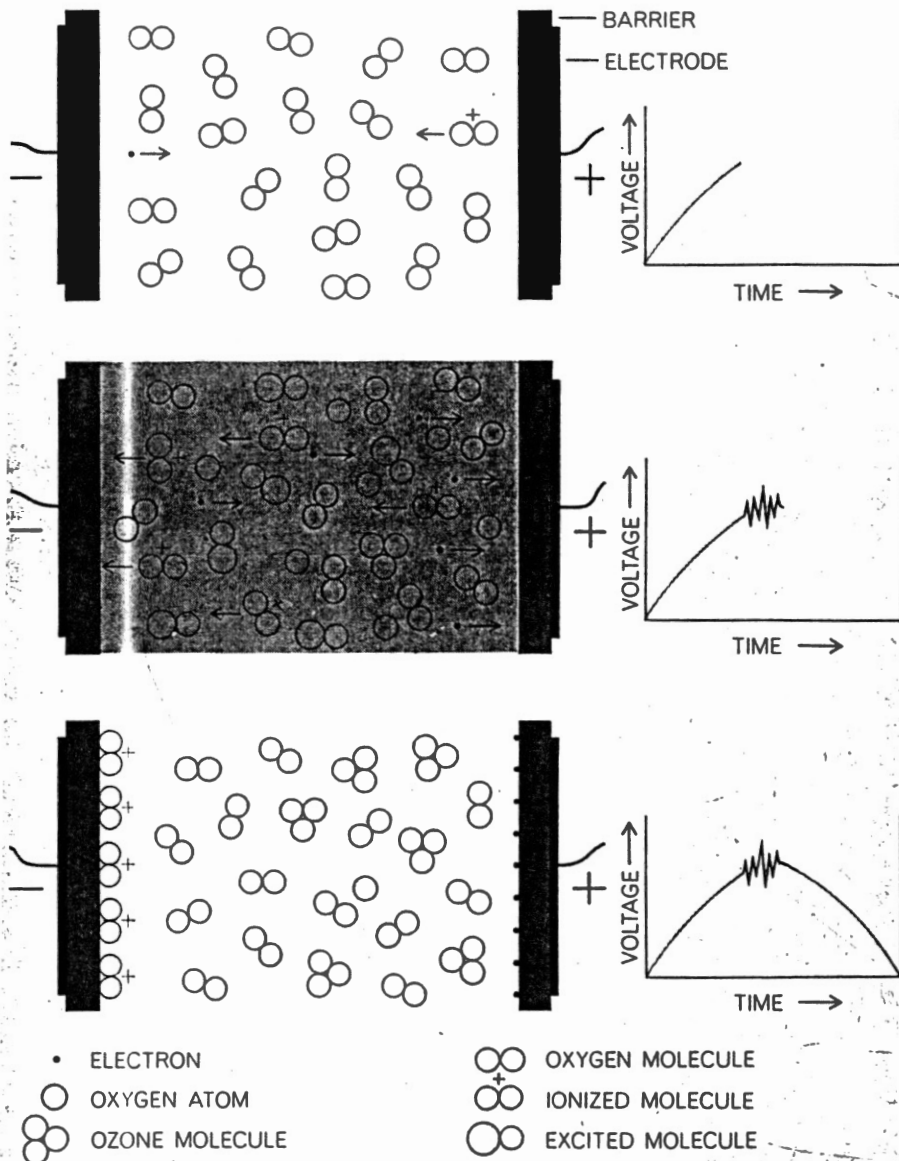
Toxic Byproducts From the Reactor

In a commercial application, air will most likely be the carrier stream flowing through the reactor due to its availability.



EFFECT OF CORONA on hydrogen is to create positive ions and free radicals. An impacting electron can knock out of a hydrogen molecule one of the two electrons orbiting the two nuclei (*top*), producing a free electron and an electron-deficient, or positive, ion. Or the impacting electron can raise the energy level of an orbiting electron (*bottom*), creating an excited molecule (H_2^*) that dissociates to form two atoms, or free radicals ($H\cdot$).

Figure 3. Mechanism for Corona Creation (1)



OZONE SYNTHESIS is a simple corona process. In the top drawing, as indicated by the oscilloscope trace (*right*), a voltage half-cycle is beginning. An electron and an ion from the previous corona burst move through the oxygen molecules toward the positive and negative electrodes respectively. In the middle drawing the corona is established. There are electrons and ions and also excited molecules that dissociate to form "free radicals" (the oxygen atoms). In the bottom drawing the electrons and ions at the electrodes have damped the corona. Most of the atoms have combined with O_2 molecules to form ozone (O_3).

Figure 4. Illustration of Corona Generation's Dependence on Frequency (1)

Formation of harmful gases are a concern with the ACPR under these conditions. The following section concentrates on these byproducts.

The predominant toxic byproducts formed with an air carrier in an ACPR are ozone, carbon monoxide and NO_x. Tevault, Chester, Simmons and Birmingham (3) studied NO_x production as a function of frequency, power and humidity. Air was used at a flow rate of 1 l/min. At low relative humidities, NO_x levels were high -- sometimes exceeding 100 ppm. However, when the inlet air was humidified to 100%, NO_x levels fell below detection limits. Thus, under these conditions, a way to handle the NO_x problem was found.

The above paper was the first to notice a resonant or optimum frequency for the ACPR. This was observed during the low humidity tests. At a fixed voltage, NO_x levels went through a maximum as frequency increased to the optimum frequency. Then, as frequency continued to rise past the optimum, NO_x levels fell back to the background level. The optimum frequency decreased at higher voltages.

Other than ozone, there have been no other research monitoring gaseous byproducts formed in the reactor. Extensive research has been done in the development of ozonizers for water purification and various other applications involving ozone, but those works have little bearing on this research.

Nitrogen Oxide Chemistry

Alternating current silent discharges have gained interest as an alternate means of air purification. One problem with the utilization of plasmas for air purification has been the formation of nitrogenous oxides, NO_x (3). As mentioned above, maximizing NO_x production from the plasma chamber will be one of the primary objectives of this research. Before trying to maximize NO_x production from the discharge, basic

chemistry and reaction mechanisms for the formation of nitrogenous oxides must be understood.

The term NO_x in air chemistry usually refers to the commonly known oxides of nitrogen. These are; nitric oxide, NO, and nitrogen dioxide, NO₂. The higher oxides; nitrogen trioxide, NO₃ and nitrogen pentaoxide, N₂O₅ are also important (21).

The main source of NO_x in the lower atmosphere is emission of NO from either soil processes or from man-made sources. An additional tropospheric source is N₂ fixation by lightning (21). Atmospheric nitrogen, N₂, is initially oxidized by lightning, an electric discharge, to form nitric oxide. Moller (45) assumed nitric oxide was formed by the reaction:



Once in the atmosphere, chemical oxidation of NO to NO₂ occurs rapidly, primarily through reaction with ozone (21):



For typical atmospheric ozone concentrations (30 ppb), NO has a life-time of approximately 1 minute with respect to the above reaction. Reaction mechanisms for NO_x production stated in this thesis come from atmospheric chemistry publications (6, 7, 18). Reaction species existing in the discharge chamber are nitrogen, nitrogen oxides, ozone and water. The discharge reactor used in this research is basically an untuned ozonizer. Past research has shown that ozone is a primary species produced in the ACPR when air is the carrier gas (3). Intuitively, if ozone is a primary byproduct from the reactor, concentrations will be in excess of the 30 ppb background concentration stated above existing in the atmosphere. Therefore, as in the

atmospheric reactions, ozone will be the primary oxidizing agent for the NO_x oxidation reactions. Water vapor is also present to precipitate nitric acid, HNO₃, as described in a previous investigation (21). All oxidation reactions involve ozone as the oxidizer. Other recombination reactions occur as shown below.

Removal of NO₂ occurs primarily via formation of nitric acid (21). The following series of reactions illustrates the path that nitrogen dioxide takes until wet deposition takes place via precipitation:



The initial product NO₃ forms nitrogen pentoxide in the reaction:



N₂O₅ reacts heterogeneously with liquid water to form HNO₃ (21). The major loss route for atmospheric NO_x is incorporation of HNO₃ and N₂O₅ into the precipitation elements followed by subsequent rain-out as nitrate ions, NO₃⁻.

The effects of nitric acid and nitrates are to be taken into account when studying the effects of air pollution in terrestrial and aquatic ecosystems. Next to SO₂, sulphuric acid and sulphates, the NO_x, nitric acid and nitrates are a threat to biota not well adapted to strong acidic conditions in soils and waters. On the other hand, the acid precipitation may add extra nutrient elements to the ecosystem. Especially, increasing depositions of NH₄⁺ and NO₃⁻ will have enhancing effects on the productivity of the ecosystem (27).

Destruction Feasibility

Although NO_x destruction was only a small part of this research, proper background investigation was mandatory to understand the destruction potential of the reactor and to deduce the necessity of experimentation. The reasons for NO_x

minimization were examined from both human health and environmental perspectives. A summary of previous destruction studies will also be presented.

Worldwide emissions of oxides of nitrogen in 1970 were estimated at approximately 53 million tonnes. As a result, the impact of air pollution is two-fold: first, by a build-up of concentrations to potentially harmful values, and second, by continuous deposition at undesired locations (30). The removal of NO_x by wet deposition is an important, yet poorly understood removal process.

Nitric acid and nitrates, the follow-up products of NO_x after oxidation and/or solution in water, when deposited as aerosols or in solutions on plants, will affect leaf tissue directly. If the pH of the solution is low enough to overcome the buffering capacity of the leaf cell cytoplasmic solution, local necrotic lesions and erosion of the cuticula could appear. Chlorosis (yellowing) of the leaf mesophyll tissue may also result. These injuries may reduce the production capacity of the plants (27). The wet deposition being referred to is commonly known as acid rain.

The adverse effects of NO_x on animals have been thoroughly investigated. Serious respiratory problems have been documented in lab animals and in humans who have been exposed to a few parts per million in a controlled laboratory environment. Morphological changes reported in a number of animal species, including mice, rats, rabbits, guinea pigs, and monkeys appeared to be most prominent in the terminal bronchiolar and alveolar duct epithelia. Exposure (to NO_x) to about 1 ppm resulted in numerous pathophysiological changes including bronchitis, bronchopneumonia, atelectasis, protein leakage into the alveolar space, changes in collagen, elastin, and mast CELSS of the lungs, reduction or loss of cilia and adenomatous changes (38).

There remains little doubt with the scientific community that exposure to nitrogen dioxide can lead to a wide variety of respiratory effects in man (31). For man, exposure to NO_x levels of 2 ppm for 10 minutes gave rise to an increase inspiratory and expiratory flow resistance. A number of authors have reported that exposure to 5

ppm for 15 minutes produced an increase in airway resistance and a decrease in the arterial partial pressure of oxygen, and carbon monoxide diffusion capacity (38).

Undoubtedly, NO_x poses significant health and environmental risk. In the past, there has been much research (21) concentrating on the minimization of NO_x from stationary and mobile combustion sources. With worldwide production of NO_x continuing to rise as the energy demands of the future are met, more effective control technologies must be investigated to minimize overall environmental impacts.

Past researchers (12, 36, 40, 41) have concentrated on the destruction feasibility of the ACPR for various airborne pollutants. These studies probed the relationship between various input plasma variables and different gases with respect to destruction efficiencies.

Much of the research reported in this section is from earlier investigations of the ACPR before the existence of an optimum frequency was known. Thus, many of the experiments were carried out at fixed frequencies of 60 Hz which is generally much lower than optimum frequencies later observed. Even at these conditions, respectable levels of destruction were obtained for small test molecules (i.e., formaldehyde), and very high destruction efficiencies were observed for large organophosphorus molecules.

Fraser, Eaton and Sheinson (32) studied the destruction of dimethyl methylphosphonate (DMMP) and trimethyl phosphate (TMP). Power to the reactor was supplied by a 16 kV, 60 Hz transformer. Table 3 lists destruction efficiencies for different flow rates and compositions.

Clothiaux, Koropchak and Moore (33) investigated the decomposition of phosphonofluoric acid methyl-1, 2, 2-trimethylpropyl ester (PFA). This compound was also used as a model to study the destruction of an organophosphorus material. Destruction results are given in table 4. Frequency was held constant at 60 Hz.

Fraser and Sheinson (34) investigated the destruction of hydrogen cyanide (HCN) and cyanogen (C_2N_2). In pure helium, both test species were removed with nearly 100% efficiency leaving a yellow solid deposit on the reactor walls (Table 5). This residue oxidized in the presence of oxygen to form carbon monoxide, carbon dioxide and nitrogen.

Neely, Best, and Clothiaux (35) studied formaldehyde destruction. The reactor frequency was held constant at 60 Hz and the voltage was varied. A mixture of 46 ppm of formaldehyde and pure oxygen was run at a flow rate of 400 cc/min in the reactor. At 12.6 kV a destruction efficiency of 40% was obtained.

Other destruction studies (40, 41, 13, 36) are presented in Table 6. The destruction efficiency indicated for each test species was the optimum attained throughout their research.

The feasibility of the ACPR as an applicable technology for the destruction of airborne pollutants has been proven, and the necessity for an efficient method of destruction of these pollutants has been shown. Future research must be undertaken to investigate more diverse destruction scenarios. Destruction of gas pollutant mixtures should be explored and scaled-up ACPR's should be built to investigate practical applications towards industrial processes.

TABLE 3

DECOMPOSITION EFFICIENCIES OF
DMMP AND TMP IN AN ACPR

Test Species	Flow Rate (cc/min)	Concentration Test Species (ppm)	Concentration Oxygen (%)	Destruction Efficiency (%)
DMMP	300	580	< 5	52
DMMP	300	580	160	72
DMMP	300	580	500	79
DMMP	300	150	< 5	99
DMMP	300	150	160	100
DMMP	1000	150	< 5	53
DMMP	1000	150	160	86
TMP	300	150	< 5	100
TMP	300	150	160	100

Source: Fraser, M. E., H. G. Eaton and R. S. Sheinson. "Initial Decomposition Mechanisms and Products of Dimethyl Methylphosphonate in an Alternating Current Discharge." Plasma Chemistry and Plasma Processing, 4(1), 1984.

TABLE 4
 DECOMPOSITION EFFICIENCY OF PFA
 IN AN ACPR

Flow Rate (cc/min.)	PFA Concentration (gm/L)	Decomposition Efficiency (%)
100	1900	> 99.6
200	1850	> 99.8
800	1950	81.5

Source: Clothiaux, E. J., J. A. Koropchak and R. P. Moore.
 "Decomposition of an Organophosphorus Material in a Silent
 Electric Discharge." Plasma Chemistry and Plasma Processing,
 4,(1), 1984.

TABLE 5
 DESTRUCTION OF HCN IN AN ACPR

Flow Rate (cc/min.)	Oxygen Concentration (ppm)	Decomposition Efficiency (%)
150	< 10	> 99.6
150	180	91.4
150	330	91.4
150	630	94.3
300	< 10	85.7
300	630	74.3

Source: Fraser, M. E. and R. S. Sheinson. "Electric Discharge Induced
 Oxidation of Hydrogen Cyanide." Plasma Chemistry and Plasma
 processing, 6(1), 1986.

TABLE 6
OTHER DESTRUCTION FEASIBILITY
STUDIES

Test Species	Optimum Destruction Efficiency (%)
Trichloroethylene (40)	> 99.9
Cyanogen chloride (41)	99.6
Hydrogen sulfide (36)	91.9
Methane (13)	75.0

CHAPTER III
EXPERIMENTAL APPARATUS, PROCEDURE
AND ANALYSIS

This chapter is divided into four sections describing various aspects of this research. Section one describes the plasma reactor chamber geometry, construction and dimensions. Section two explains the discharge system and instrumentation used for electronic data acquisition. Section three describes the flow schematic of the entire system. Section four outlines experimental procedures and data analysis techniques used throughout this research.

Reactor Geometry and Dimensions

The primary piece of experimental apparatus used in this research is an alternating current plasma reactor (ACPR), which is basically a combination of a capacitive and an inductive device. The reactor, coupled with a variable power source, both of which will be described later, provide the necessary conditions for an effective plasma to be generated.

The discharge reactor was fabricated using Pyrex glass and consists of two concentric cylinders forming an annulus through which the reactant gas flows. The Pyrex glass is Corning code 7440 chemical-resistant borosilicate glass with a dielectric constant of 4.6 at 25 °C (12). Figure 5 illustrates the reactor geometry. Two electrodes were situated in/around the reactor to create an electric discharge, or plasma, in the annulus. The inner electrode consisted of 40 mesh copper sheet wrapped

in a cylinder and inserted inside the inner glass cylinder. The outer electrode consisted of a molybdenum wire (1 mm diameter) wrapped, 17 times, around the outside of the outer glass cylinder. The electrode arrangement has two purposes: First, having the electrodes each exterior to the annulus, there can be no corrosion or electrode fouling due to gaseous interaction with the electrodes. Second, the glass barrier between each electrode allows the current to diffuse into a uniform glow in the annulus. The barrier interrupts the conductive path and allows only an incomplete breakdown of the gas: instead of a hot localized arc there is a cooler, diffuse glow between the electrodes (1).

Discharge System

The electrical system is an impedance-changing circuit. Power is supplied through a voltage transformer (California Instruments Model 161T) with a plug-in California Instruments Series 800T Oscillator. Instrument output range was from 0 to 120 volts rms and 40 to 5000 Hz. The California Instruments power source regulates the voltage from the 110 volt wall socket. This voltage is the primary voltage. In order to generate a plasma, a very strong electric potential must be applied across the electrodes of the discharge reactor, requiring upwards of 15,000 volts (1). This voltage step-up, the secondary voltage, was attained by using a Jefferson Electric luminous tube transformer. The secondary voltage of the transformer can be tuned by varying the output frequency of the primary voltage. The oscillator used to vary frequency is a type of Wien-bridge and produces a nearly perfect sine wave with less than 1% distortion from 20 to 200

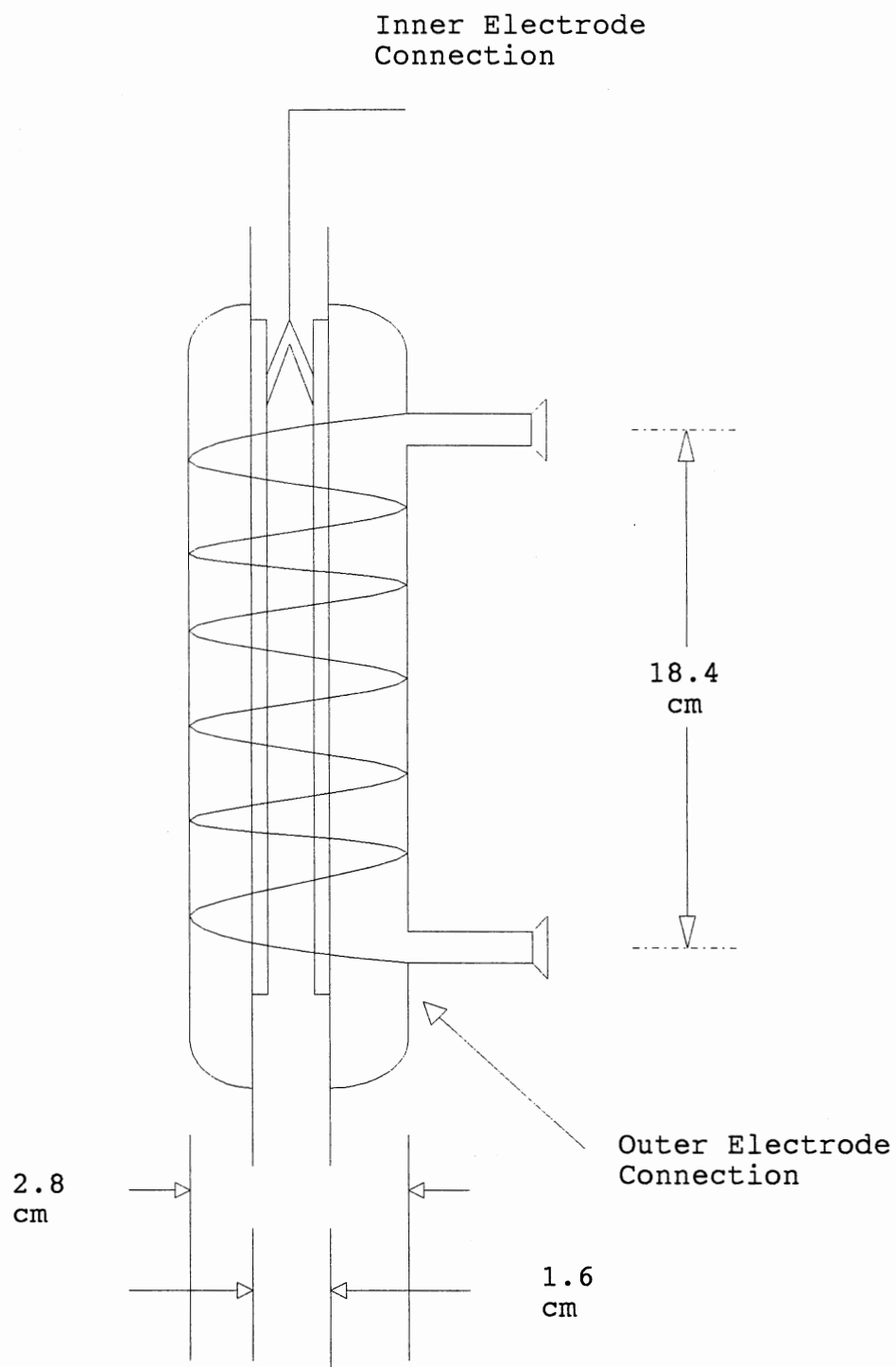


Figure 5. Alternating Current Plasma Reactor (ACPR)
 Annular Volume = 74.78 cm^3

Hz. The iron-core transformer (Jefferson Electric Co.) which was used is a luminous tube, high power factor transformer with a midpoint grounded secondary. The output from one winding is positive-going with respect to ground, while the output from the other is negative-going, and vice versa. The total output voltage from the windings is the sum of the outputs from each. The rating of the transformer is 15 KV and 60 mA for a primary voltage of 120 at 60 Hz.

The primary current was measured using a meter shunt rated at 1.5 ampere which had an equivalent voltage drop of 50 mV. A digital multimeter (Fluke Model 8050A) was used to measure the potential across the shunt. The primary voltage was read off the power amplifier panel. For the measurement of secondary voltage, a Simpson AC high voltage probe was used in conjunction with a Simpson 260 Series 7 multimeter.

Experimental Apparatus

A schematic of the apparatus is shown in Figure 6. Flow rate and humidity were regulated using a Linde FM4575 Mass Flow Meter/Flow Controller. The mass flow controller provided control of multiple flow rates by using separate mass flow control modules. Modules were calibrated with dry tanked breathing air. Actual individual flow rates through each module were calculated from calibration regression curves then added to obtain total flow. Module one, Linde Mass Flow Control Module Model 10C-202-4124, controls the flow of dried air. Stream one passes through a gas drying chamber filled with Dry Rite, CaSO_4 , then combines 20 in. downstream with stream two. Flow through module two, Linde Mass Flow Control Model 9C-202-4124, passes through a water bubbler consisting of two 500 ml. Erlenmeyer flasks filled with water, then a 250 ml. Erlenmeyer flask serving as a condensation trap.

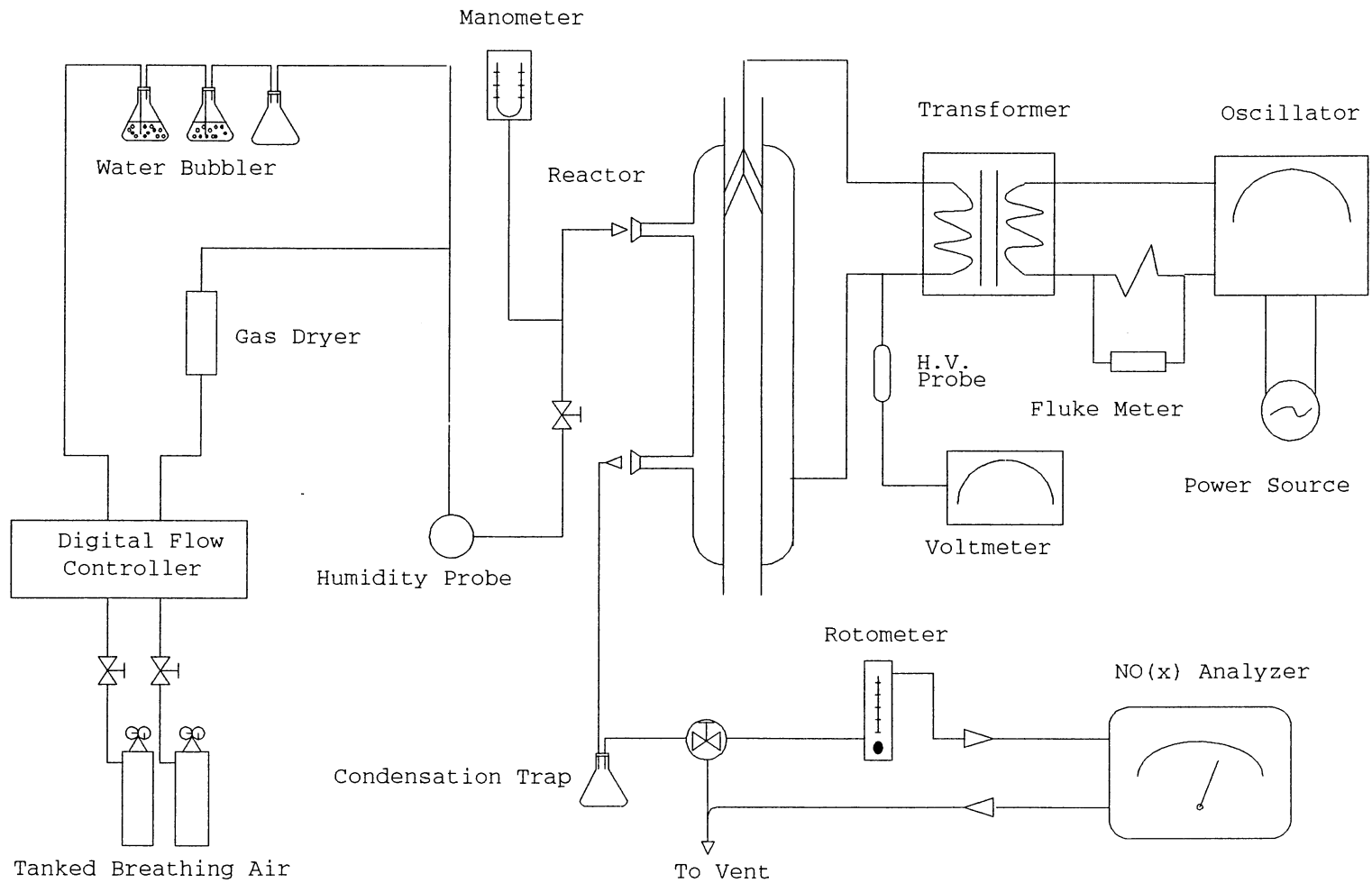


Figure 6. Schematic of Experimental Apparatus

All flasks were partially submerged in a room temperature water bath so small variations in atmospheric conditions did not vary humidity. Controlling the flow ratio of stream one to stream two allows for the reliable variation of humidity with a consistent total flow rate. Humidity was monitored using a Davis Instruments Model DTH-1 Digital Hygrometer/Thermometer.

Reactor pressure was monitored using a mercury manometer to ensure approximate atmospheric conditions existed in the reactor chamber. The manometer was located 6 inches before the inlet of the reactor.

On the outlet side of the reactor a condensation trap was installed 7 inches downstream of the outlet. The condensation trap, shown in Figure 7, was placed in a 1000 ml. Erlenmeyer flask partially filled with water and the flask was submerged in an ice bath to ensure a large temperature gradient to effectively capture all condensate formed in the reactor due to gas stream humidity.

A three way valve was used to divert flow to the vent when NO_x calibration was necessary. A double check for total flow rate was provided by means of a Fischer Mark III type rotometer Cat. No. 448-225. The rotometer was calibrated with dry breathing air. Total flow values calculated from Mass Flow Module calibrations were checked against known rotometer settings to have a constant check for system integrity. After passing through the rotometer, the stream flows into the primary analysis tool used in this research. Gas analysis was performed on a Thermal Electron Chemiluminescent NO_x Analyzer. This device utilizes the chemiluminescent reaction between nitrogen dioxide and ozone to measure NO_x concentration. The NO_x analyzer was always on-line providing a continuous reading of parts per million (ppm) concentration being produced from the reaction chamber. After analysis the stream is exhausted from the analyzer and directed to the vent for discharge.

Most flow lines are welded stainless 1/4" x 0.035" T304 tubing. For safety, flow lines connected directly to the reactor chamber are 1/4" x 1/16" Tygon tubing.

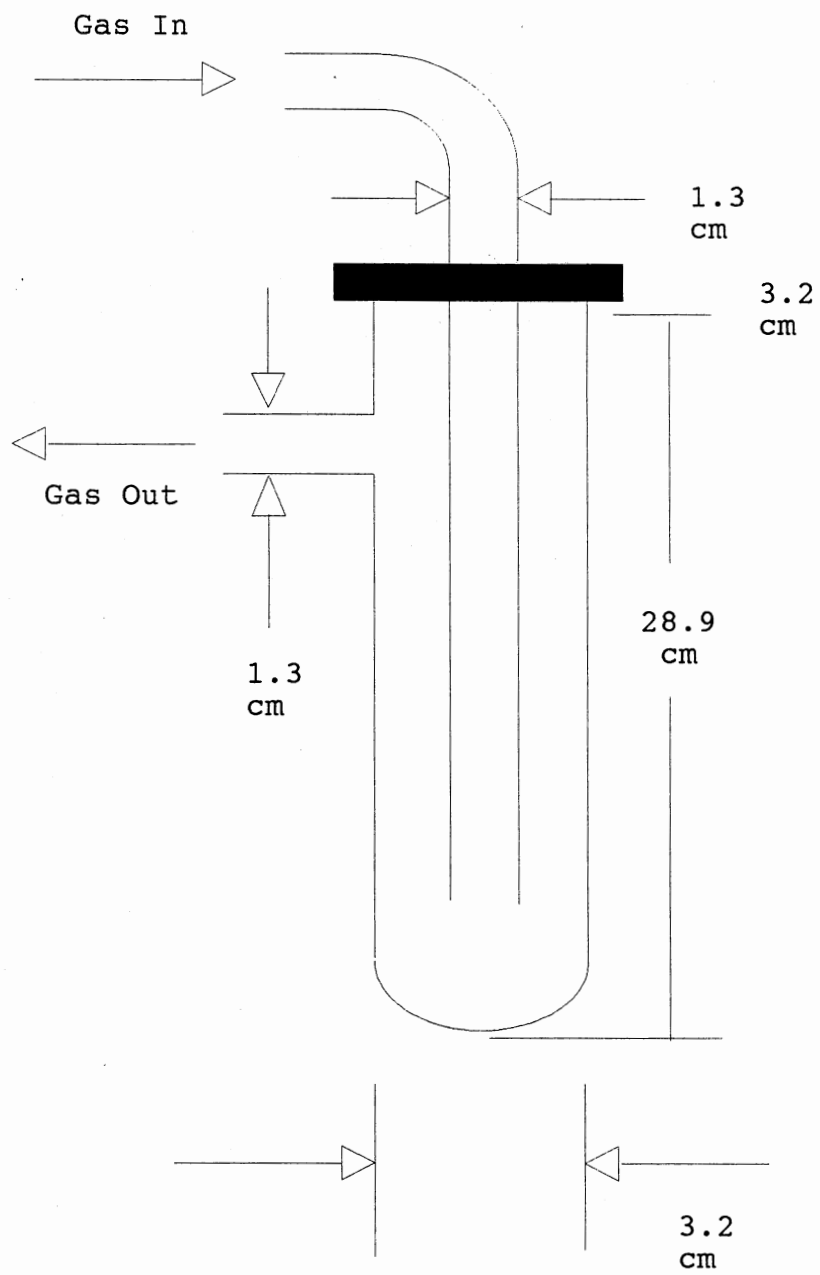


Figure 7. Cold Trap Condensing Chamber

Tygon tubing was used instead of stainless to ensure isolation of electric currents. The reaction chamber was mounted on a dowel rod with clips having rubber contact points for added electronic isolation. The chamber and discharge system were located inside a hood with a retractable glass window. The power source and indication instruments were located exterior to the hood to allow the operator to control input plasma variables and to safely read instrumentation.

A pictorial representation of the experimental apparatus used in this research is shown in Figures 8 - 13.

Experimental Procedure and Analysis

The following section briefly describes experimental design, procedure, and analysis methods used in this research.

Reactor Optimization

Before any data regarding the oxides of nitrogen produced from the plasma chamber could be obtained a basic understanding of the plasma with respect to input electrical variables had to be fully investigated. For reactor optimization, dry breathing air was the reactant gas. Air was allowed to flow through the reactor for 3 - 5 minutes at the desired flow rate without any electric potential applied across the electrodes. This ensured all optimization testing input flow variables would be consistent. The power supply was turned on and set at the desired primary voltage. While keeping the primary voltage constant, frequency was varied from 60 Hz to 1500 Hz in increments of 50 Hz. Near the optimum, incremental changes were reduced to 10 Hz, to accurately pinpoint optimum. At each frequency increment, primary current and secondary voltage were recorded. Primary power was calculated

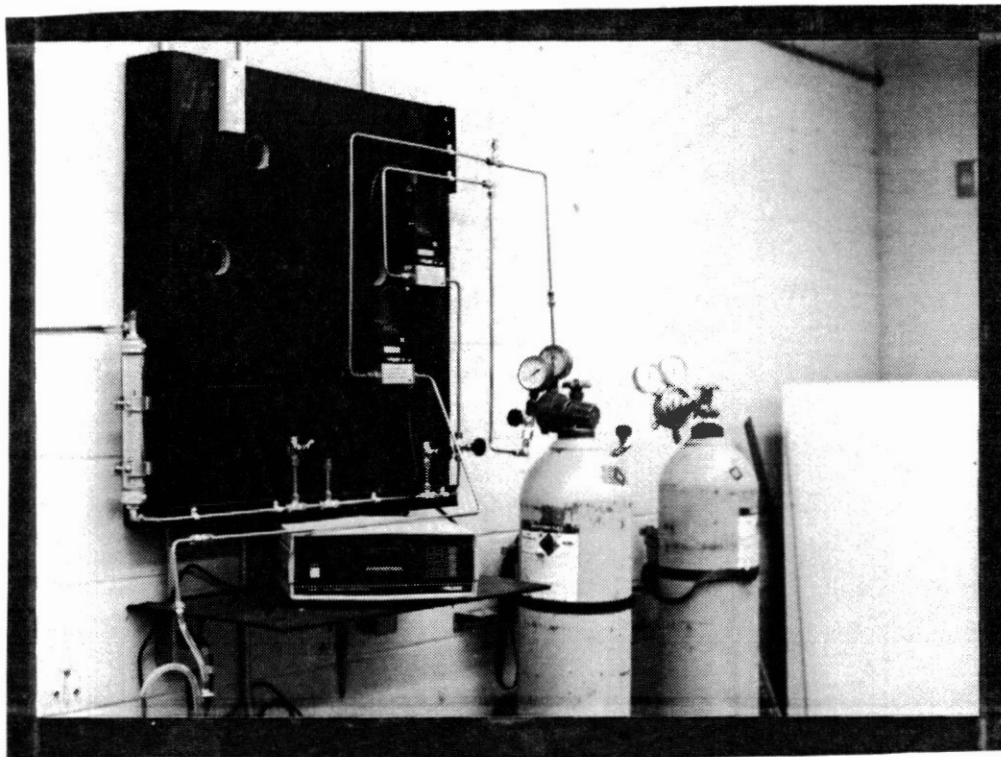


Figure 8. Breathing Air Streams 1 & 2, Flow Control Modules and Gas Dryer

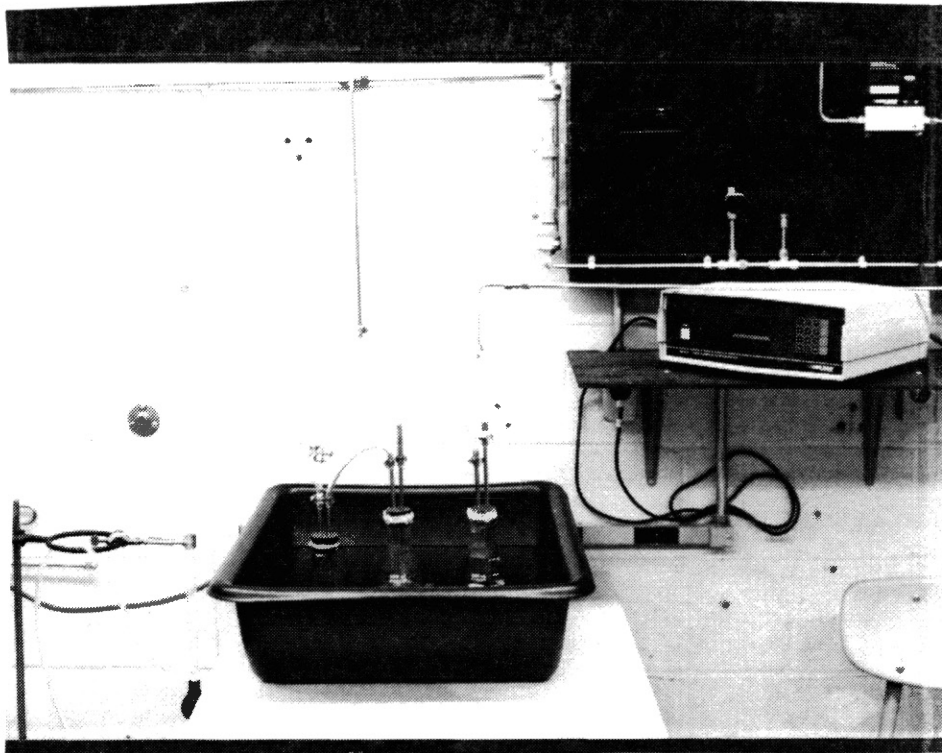


Figure 9. Humidity Source and Junction for Streams One and Two

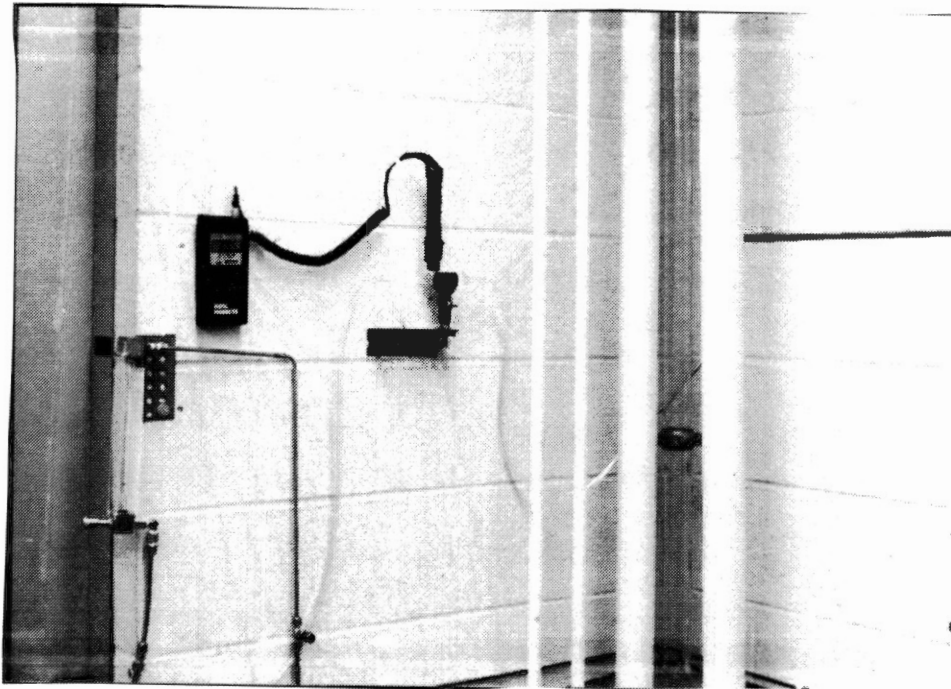


Figure 10. Humidity Probe and Monitoring Port

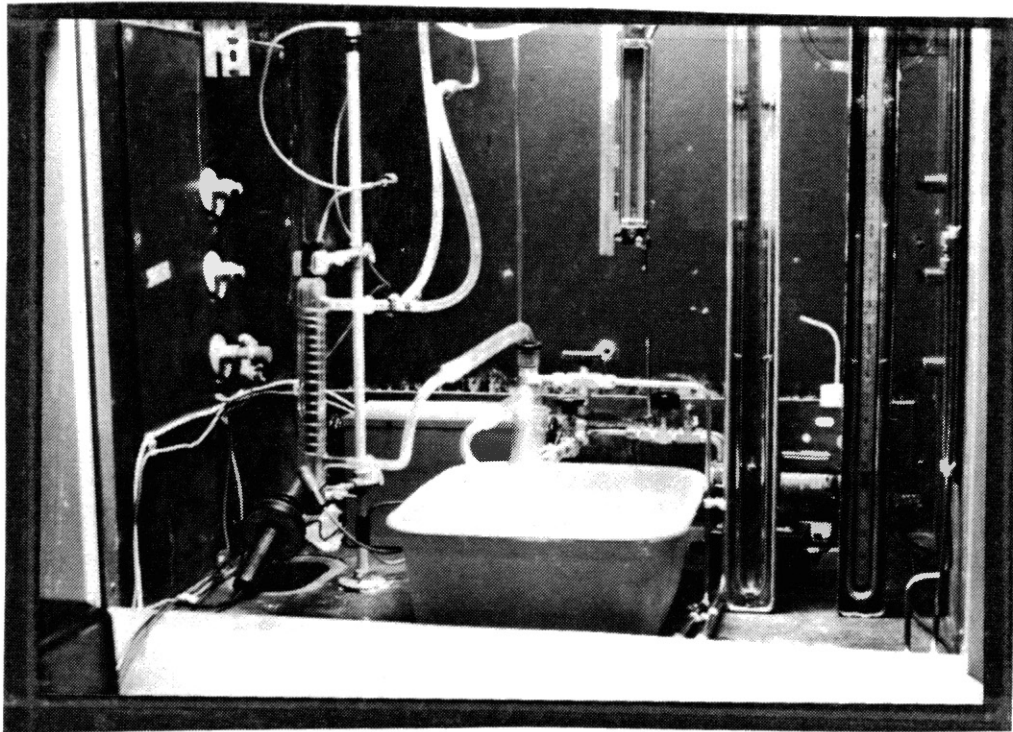


Figure 11. Alternating Current Plasma Reactor and Apparatus Under the Hood

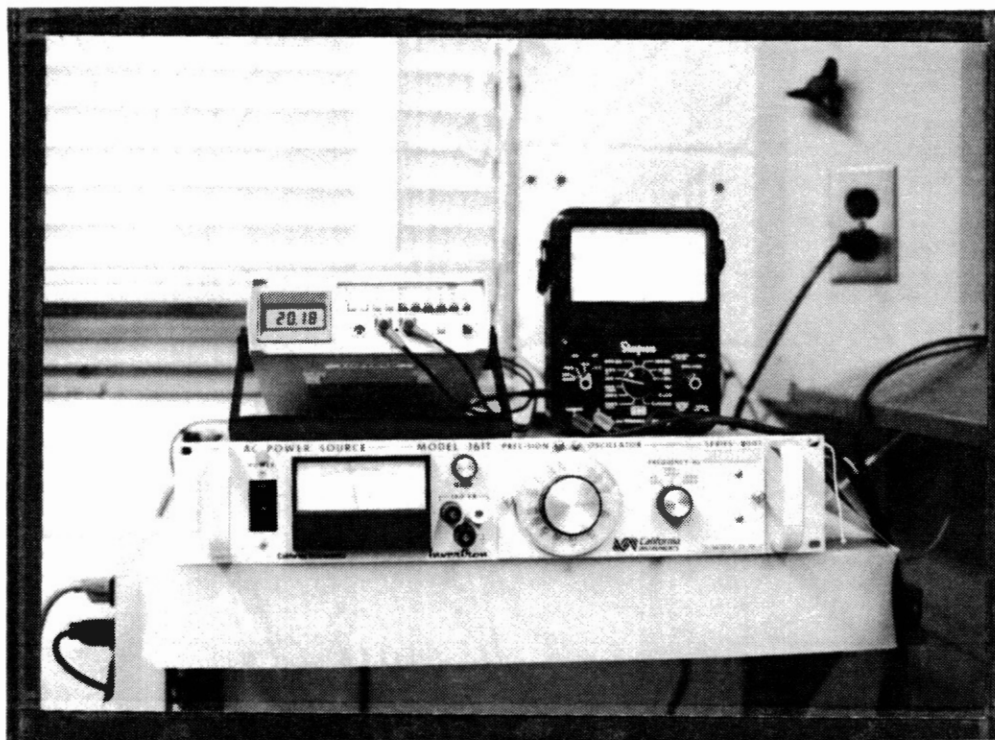


Figure 12. Discharge System and Electrical Monitoring Apparatus

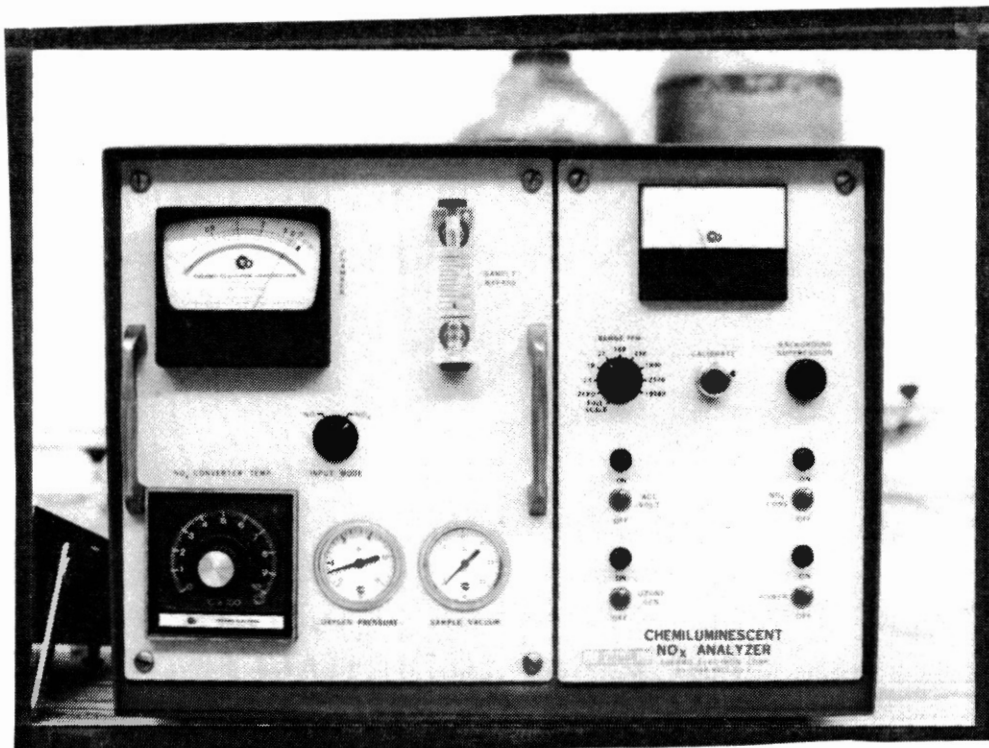


Figure 13. Chemiluminescent NOx Analyzer

by multiplying primary voltage and primary current. This procedure was repeated for dry air at primary voltages of 20, 30, 40, 50 and 60 volts. Since humidity variation is a primary concern, reactor optimization was rechecked at a relative humidity of 45% and a primary voltage of 60 volts. The dry and humidified optimization curves were compared to see if humidity appreciably changed the electrical characteristics of the plasma.

Experimental Design

Experiment design refers to the order of variable testing. This section will provide a brief overview to the approach that was taken to understand the effects that targeted variables have on the production of NO_x from the discharge reactor. Initially, reactor optimization was performed as stated above.

NO_x production testing procedure allowed for the variation of the following: primary voltage, frequency of that voltage, reactor residence time, and relative humidity. To vary each variable with respect to every other variable would have been redundant and inefficient. Therefore, a logical testing sequence was conceived to attain the most efficient use of experimental time.

First, primary voltage was varied from 20 to 60 volts. At each voltage increment, optimum frequency for that voltage was used to ensure maximum plasma power input, and NO_x production at each voltage was recorded. The primary voltage that maximum NO_x production occurred at was noted and further tests were all conducted at that primary voltage.

To be sure that maximum NO_x production occurred at the optimum frequency for each voltage, production was monitored after changing the frequency to values above and values below the optimum setting. This resulted in the deduction that maximum production did in fact occur at the optimized setting.

To see what effect flow rate had on NO_x production, gas flow rate was varied and NO_x production noted. Production vs. flow rate tests were all conducted at the same optimized primary voltage setting mentioned above (primary voltage and frequency remained constant). This provided a consistent plasma power input so that an accurate relationship could be found between reactor residence time and NO_x production.

Relative humidity of the incoming air stream was the last variable targeted for testing. All other experiments were run with dry air. The same optimized setting used for flow rate variation testing was also used for this testing segment. Flow rate was kept constant, consistent plasma power input and flow rate were also maintained so that an accurate relationship could be found between relative humidity and NO_x production.

Additional Testing

Additional testing was undertaken to investigate the feasibility of using the ACPR as a destruction mechanism for NO_x, and to gain insight into the proposed chemical reactions involving NO_x occurring in the discharge chamber.

The pilot investigation regarding the destruction of NO_x by the plasma chamber attempts to illustrate the ACPR is an effective method for eliminating the oxides of nitrogen from a gas stream. If successful, further research would be required to fully understand the potential that the discharge reactor will have as an effective way to minimize NO_x emissions from stationary and mobile combustion sources. Destruction tests were performed using a nitric oxide, NO, standard of 7459 ppm balanced in nitrogen. Analysis was done on the Thermal Electron NO_x analyzer.

In an attempt to validate the chemical reactions proposed in earlier sections detailing the oxidation mechanisms of atmospheric nitrogen to its various oxides,

condensation collected in the cold trap and NaOH solution samples after having the post plasma gas stream bubbled through it were analyzed. The tool of analysis was a Dionex Series 2000i/SP Ion Chromatograph with an Ionpac A54A-SC Analytical Column (P/N 043179). The column detects Fluoride, Chloride, Nitrite, Bromide, Nitrate, Phosphate, and Sulfate. Experimental results were obtained through comparison with a standardized concentration curve prepared for the column in question. Column response can be found in Appendix E. A Hewlett Packard 3380A Integrator was utilized as the printing apparatus. This experimentation was necessary to approximate what other oxides of nitrogen, besides NO_x, are produced as byproducts in the plasma chamber.

The following subsections will briefly outline procedures used for monitoring production with respect to the targeted variables.

Primary Voltage Variation

NO_x production testing as a function of primary voltage was investigated to determine if power input to reactor had an influence on NO_x production. Incoming gas stream conditions throughout primary voltage variations were kept constant. Dry breathing air was passing through the reactor at a rate of 118 ml/min.

Experimental procedures are summarized as follows:

1. Power supply was turned on and the primary voltage was set. Dry air passed through the reactor at the specified flow rate.
2. The secondary voltage of the transformer was raised to the optimum reactor setting for that primary voltage by varying frequency.
3. Plasma was given ample time to stabilize. Steady state was reached at a time when NO_x production varied no more than +/- 5% over the course of an hour.

4. NO_x production, primary current, and secondary voltage were recorded.
5. Steps (2), (3) and (4) were repeated for the different primary voltages.

Frequency Variation

Frequency variation was performed mostly at a primary voltage of 60 V. At 60 volts, the discharge became stable after approximately 20 minutes.

Experimental procedure is generalized as follows:

1. Start-up procedure was the same as shown in steps (1) & (2) of the primary voltage tests.
2. Frequency was changed, primary current and secondary voltage were recorded.
3. Discharge stability was determined as described in step (3) of primary voltage variation.
4. NO_x production was noted.
5. Steps (2), (3) & (4) were repeated to make sure results were conclusive at the set primary voltage.

Flow Rate Variation

Flow rate variations were performed mostly at a primary voltage of 60.

Experimental procedures are summarized as follows:

1. Start-up procedure was the same as shown in steps (1) & (2) of the primary voltage tests.
2. Residence time was changed by varying the gas flow rate to the reactor chamber.
3. Discharge stability was determined as described in step (3) of primary voltages variation.

4. NO_x production, primary current, and secondary voltage were recorded.
5. Steps (2), (3), & (4) were repeated for the different residence times.

Relative Humidity Variation

Relative humidity variation was performed mostly at a primary voltage of 60.

Experimental procedures are generalized as follows:

1. Start-up procedure was the same as shown in steps (1) & (2) of the primary voltage tests.
2. Relative humidity was changed by varying the ratio of stream 1 to stream 2 while maintaining a constant total flow rate.
3. Discharge stability was determined as described in step (3) of primary voltage variation.
4. NO_x production, primary current, and secondary voltage were recorded.
5. Steps (2), (3), & (4) were repeated for the different relative humidities.

Additional Testing Procedures

Destructive Testing. Destructive testing was based on a percent removal investigation. The known standard of 7459 ppm was used to calibrate Flow Module #1 and passed through the plasma chamber with no potential applied at the desired flow rate. The gas flowed for 5 minutes to allow any air to be purged from the system. The NO_x analyzer was calibrated to the standard, then the potential was applied. All destruction tests were performed at the optimized 60 volt setting. Ample time was allowed for the plasma to become stable, see step (3) from primary voltage variation. The NO_x concentration was then recorded. The above procedure was repeated for different residence times by varying the flow rate. Destruction efficiency was calculated as a percent removal. See sample calculations in Appendix A.

Chemical Reaction and Mechanism Validation. Validation of the proposed chemical reactions and mechanisms was accomplished by analyzing condensation and bubbled samples with the Dionex Ion Chromatograph explained above.

Condensate was allowed to collect for approximately 2 weeks. Condensate was removed from trap and sample preparation was done as dictated in the Dionex Chromatograph Manual. The sample was injected into the Ion Chromatograph and results were deduced as shown in Appendix A.

A bubbler was constructed of a 250 ml erlenmeyer flask and inserted into the experimental apparatus immediately before the NO_x analyzer. The flask was filled with a 0.0124 M solution of NaOH and the post reactor gas flow was bubbled through the solution for 5 hours. Sample preparation was done as dictated in the Dionex Chromatograph Manual. The sample was injected into the Ion Chromatograph and results were deduced as shown in Appendix A. This test had to be done due to the volatile nature of nitrite. When allowed to sit for weeks, nitrite, NO₂⁻ tends to be volatilized and/or converted to nitrate, NO₃.

CHAPTER IV

REACTOR OPTIMIZATION

Before any of the primary objectives of this research could be investigated, plasma response with respect to input electrical conditions must be understood. By conducting these experiments, trends in plasma generation with respect to certain variables could be realized.

Results and Discussion

The results are presented in a graphical form and discussed in the following sections. Optimization test data with all fixed conditions are tabulated in Appendix B.

Power Dependence on Frequency and Primary Voltage

Figure 14 shows the relationship between power input to the reactor and frequency at different primary voltages. All tests were conducted with dry air. Dry air corresponded to an indicated relative humidity of 9.7%. The Davis Instruments probe was accurate from 20 to 90%, so an exact water vapor content at the low humidity levels was not available. The power input initially increases with an increase in frequency. At a certain value of frequency for a particular primary voltage, reactor power goes through a maximum and then begins to decrease with increasing frequency. This peak is called the optimum condition. The reason for the optimum

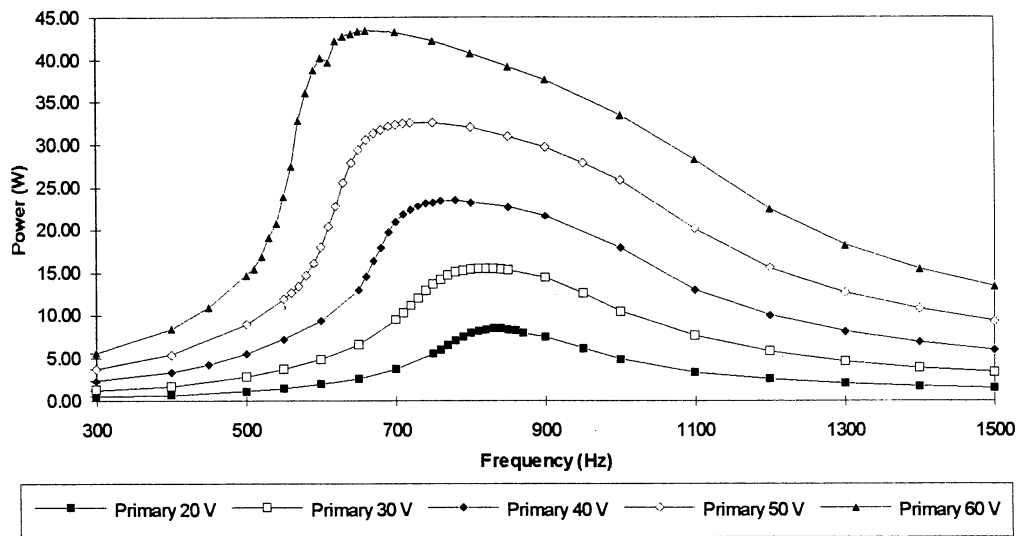


Figure 14. Dependence of Reactor Power Input on Frequency for Air at Fixed Primary Voltages and 118 ml/min

condition is believed to be a result of the secondary electrical circuit loading on the transformer. Transformers are basically inductive devices and consist of two sets of windings. When a capacitance generating circuit is connected to the secondary side of a transformer, a frequency exists where the capacitance of the circuit is equal to the inductance of the transformer. This condition is called resonance, and at this point secondary voltage goes through a maximum (42). Power input to the plasma and secondary voltage peak at the optimum frequency showing approximately the same relationship with respect to frequency, see Figure 15. Power input and secondary voltage both go through their maximum at the optimum frequency.

It was observed that as primary voltage increased, the value of the maximum power input increases. The value of optimum frequency decreases as primary voltage increases. Thus optimum frequency reveals the frequency range to be expected for operation of a particular capacitive discharge reactor system. Previous research (12, 14, 36) yielded similar optimized conditions for various discharge reactors.

Plasma Behaviour with Respect to Humidity

Figure 16 illustrates the effects of humidity on plasma reactor behavior. The optimizations were both conducted at 60 volts. One was done using dry air, the other was done with the air humidified to 45% relative humidity. As the graph shows, humidity has negligible effects on plasma behavior.

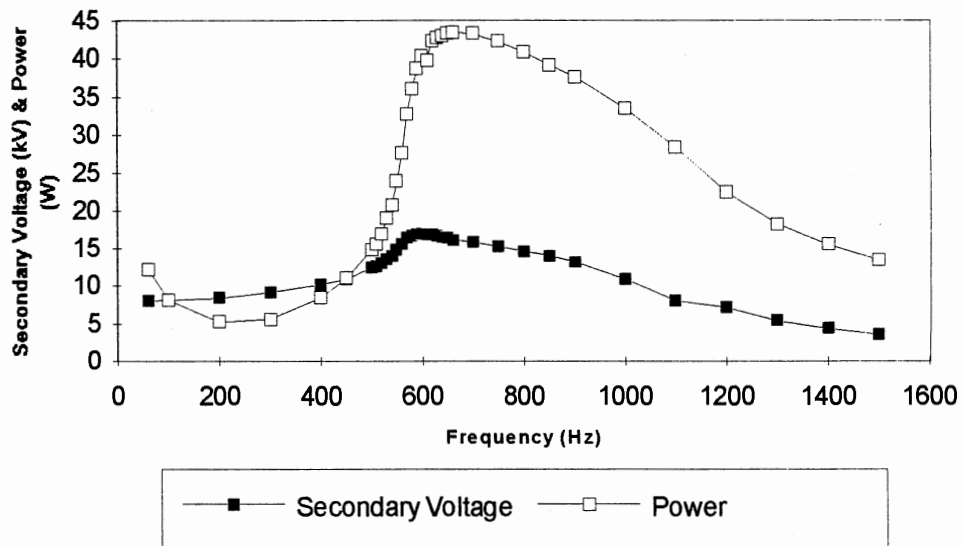


Figure 15. Relationship of Power and Secondary Voltage to Frequency at a Primary Voltage of 60 and 118 ml/min

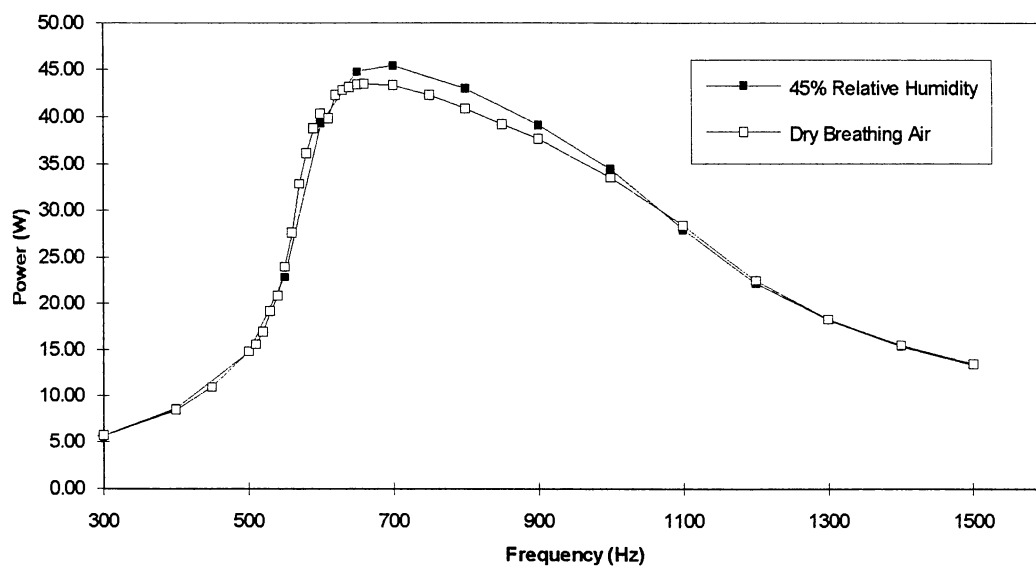


Figure 16. Effect of Humidity on Plasma Behavior

CHAPTER V

NO_x PRODUCTION TESTS

As mentioned earlier, the primary objective of these experiments was to determine the effectiveness of the ACPR as a NO_x production mechanism and how the production is affected by primary voltage, frequency, flow rate and humidity variations. After production potential was deduced, target variables were manipulated to maximize NO_x produced in the plasma chamber. The results of these experiments are presented in a graphical manner and are discussed in the sections below.

The maximum NO_x production achieved in the following experiments was 1700 ppm. The range of production obtained with respect to the various target variables is quite large, from 3 to 1700 ppm. Production test data can be found in Appendix C.

Preliminary Testing Realizations

Initially, to determine long term plasma stability, NO_x production was monitored at an optimized primary voltage, and consistent flow rate for upwards of 48 hours. Yellowing and condensation were noticeable in the Tygon Tubing on the outlet side of the discharge chamber. These undesirable residues were found to accumulate over time. At low primary voltages (20 & 30 volts) practically no buildup or condensation was noticed over a continuous testing span of 44 hours. As the voltage increased from 40 to 60 volts, tubing discoloration and condensate deposition

occurred progressively faster. These phenomena were undesirable because they erroneously increased the NO_x production from the discharge chamber indicated by the NO_x analyzer. This was proven by letting the discharge chamber run at 60 volts (optimized) until an appreciable amount of condensate had accumulated in the tubing, then shutting off power to the reactor. At the time of power shut down the NO_x concentration was 580 ppm. The tanked breathing air had a background concentration of approximately 3 ppm NO_x. After power was shut off, gas was allowed to flow for approximately 15 minutes to provide ample time to clear the lines of post plasma gas. The NO_x concentration indicated did not decrease past 300 ppm. Tygon Tubing on the outlet side of the reactor was replaced with clean, new tubing and the NO_x concentration immediately went down to the expected background level mentioned above. Initial approximations for the yellowing was oxidation of the tubing due to ozone. The same discoloration has been noted in the operation of ozonizers having Tygon Tubing connected to the outlet side of the reactors (43). The condensation was hypothetically identified as nitric acid, HNO₃.

The only reactants flowing through the plasma chamber were breathing air (approximately 79% nitrogen and 21% oxygen), and water vapor, therefore, these are the only species available for reaction in the discharge chamber. To test the condensation hypothesis, the pH of the condensate was approximated. A beaker was filled with 20 mls of tap water and the pH was tested. The pH of this water was 6.68 (meter was not standardized). Through the condensate laden tubing, 3 mls of the same tap water was allowed to trickle into the partially filled beaker. The addition of the 3 mls decreased the pH to 0.72 in 8 seconds. These results, which are further validated later, indicate the condensate as extremely acidic.

The condensation problem was eliminated by installing a cold trap immediately downstream of the discharge chamber's outlet. This cold trap removed the water vapor from the gas stream and can be seen in Figure 7.

Dependence of NO_x Production on Primary Voltage

Figure 17 shows the production trend of NO_x with respect to primary voltage in concentration units of parts per million (ppm). As in previous research (3), NO_x production increased as primary voltage increased.

The directly proportional relationship between primary voltage and NO_x production stems from reactor power input. As optimized primary voltage increases, plasma power input also increases, see Figure 14. Keeping all gas flow variables constant and varying the optimized primary voltage, effectively only changed the power input per unit volume of gas flow. The added energy available for plasma chemical reactions, promotes a higher power discharge. This added power yields increased decomposition of reactants, resulting in more recombination byproducts, and therefore, more NO_x.

In previous destruction studies utilizing the ACPR (13, 36), increased destruction efficiency was reported as optimized primary voltage increased. These results support the hypothesis cited above explaining why NO_x production increases with increased primary voltage.

Dependence of NO_x Production on Frequency

Figure 18 shows the effect of frequency on NO_x production. These tests were conducted keeping the primary voltage and flow rate constant. These results agree with previous research (3). Production was a maximum at optimized conditions, and decreased on either side of the optimum frequency. These results can also be tied into the plasma power input hypothesis stated above. As the frequency approaches the optimum, power is also approaching its' maximum for that primary voltage, see

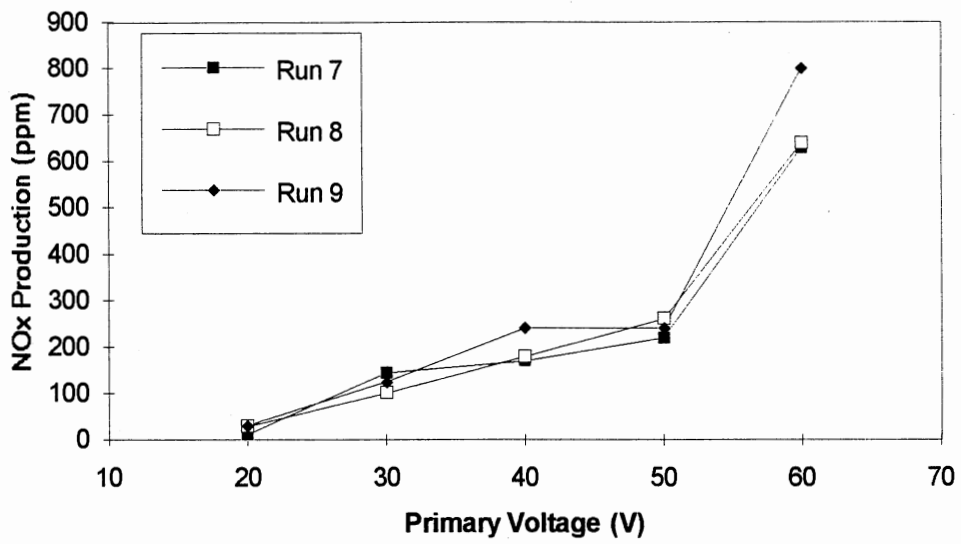


Figure 17. NOx Production With Respect to Primary Voltage
Dry Air @ 118 ml/min

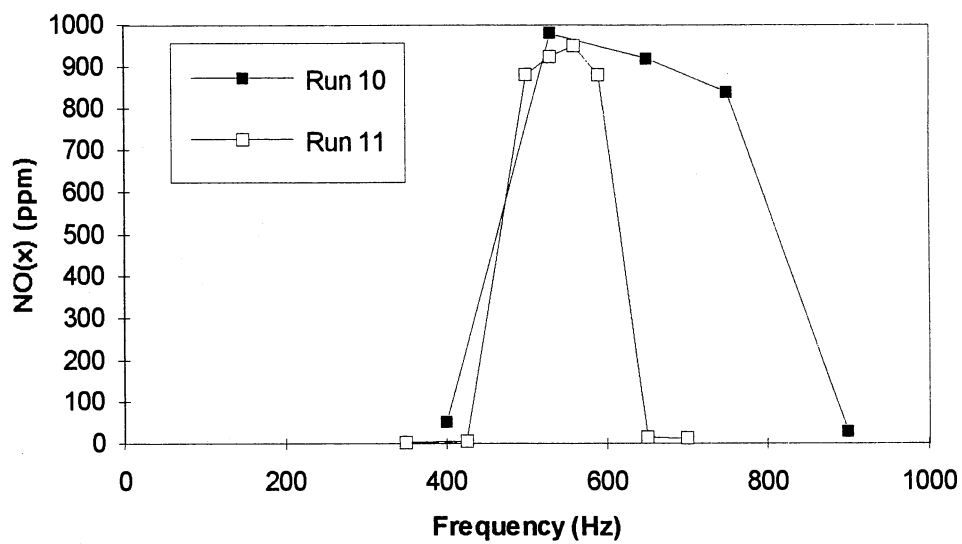


Figure 18. NOx Production With Respect to Frequency at 60 volts. Dry Air @ 118 ml/min

Figure 14. The direct relationship between power input and NO_x production is the same, but the independent variable is frequency as opposed to primary voltage.

Dependence of NO_x Production on Flow Rate

Figure 19 shows the relationship between NO_x production and flow rate. These tests were conducted using the dried tanked breathing air flowing through the discharge chamber at an optimized 60 volt setting. An inversely proportional relationship was discovered. As flow rate increases, NO_x production decreases.

Past destructive studies (13, 36), have shown that destruction efficiency decreases as flow rate increases. Again, destruction or decomposition, is the precursor to the formation of NO_x as was discussed in previous sections. As flow rate is increased, the residence time decreases which decreases the amount of energy that can be imparted to the reacting molecules. The less energy imparted to the reactants, the less decomposition, and of course the less recombination of the byproducts forming NO_x.

Dependence of NO_x Production on Relative Humidity

Figure 20 shows the variation of NO_x production with respect to relative humidity. All tests were performed at the optimized 60 volt setting with a flow rate of 146 ml/min. NO_x production at low level humidity (dry air) is 540 ppm. This agrees with previous findings in this research. As the air stream's water vapor content is increased, NO_x production increases to it's maximum of 1700 ppm at 35% relative humidity. If relative humidity is further increased, NO_x production rapidly drops to the background level in the tanked breathing air, 3 ppm.

The sharp peak at 35% relative humidity shows that the NO_x production is not a one dimensional phenomenon. To have a maximum occur as shown, there must

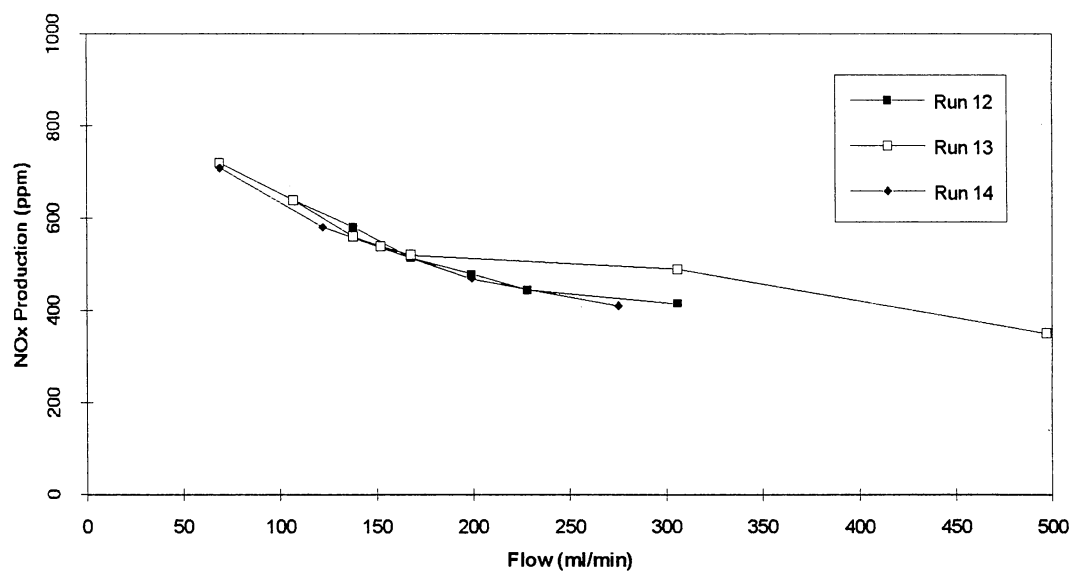


Figure 19. NOx Production with Respect to Flow Rate at 60 volts Dry Air

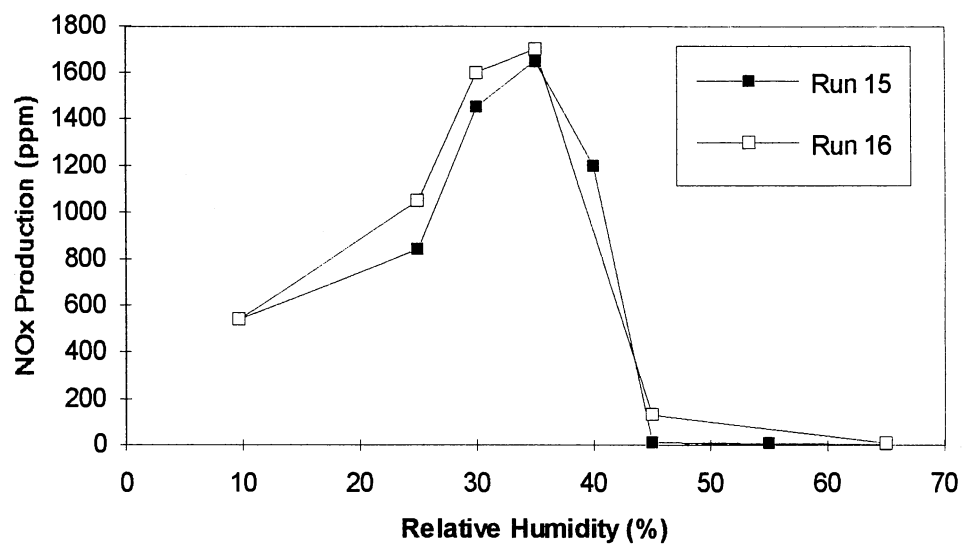


Figure 20. NOx Production With Respect to Relative Humidity at 60 volts Flow Rate 146 ml/min

be competing reactions occurring in the discharge chamber. As humidity is increased from 10 to 35%, the added water vapor introduced somehow increases the NO_x formed in the discharge chamber from 540 to 1700 ppm. Above 35% relative humidity, the enhanced production is choked off and production rapidly drops to 3 ppm.

A possible explanation for this behavior stems from a combination of two things. First, the difference in bond energies of nitrogen, N₂, and water. And second, the reaction of the oxides of nitrogen formed in the plasma chamber not detected by the NO_x analyzer with radicals formed by the decomposition of water. The NO_x analyzer ultimately only detects NO and NO₂. Various oxides of nitrogen may be formed in the reaction chamber, but when the sample enters the analyzer the gas passes through a 600 °C conversion chamber. This exposure to extreme heat may convert some higher oxides to the more basic nitrogen oxides. For example, N₂O₄ may be broken down to NO₂ and NO₂.

Qualitative analysis has never been done to determine all of the oxides of nitrogen produced by the ACPR. The following sections are hypothetical and require further investigation to prove or disprove. Based on inorganic chemical reactions that are known to occur naturally, an approximation of what could be happening in the discharge chamber with respect to known constraints is as follows:

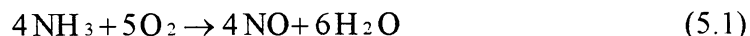
Possible Reasons for NO_x Increase

The NO_x Analyzer Detects: NO and NO₂

The NO_x Analyzer Doesn't Detect: N₂O, N₂O₂, N₂O₃, NH₃
NO₂⁻, NO₃⁻

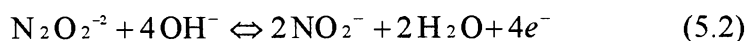
If any of the above listed compounds not detected by the analyzer

recombines with a radical resulting from the decomposition of water and forms either NO or NO₂, then the indicated concentration of NO_x would increase. The radicals resulting from the decomposition of water are H, OH, H⁺ and OH⁻. Moeller (45) lists the following naturally occurring reactions involving various oxides of nitrogen:



The above reaction represents the equilibrium of NH₃ and O₂ with NO and H₂O possibly existing in the plasma chamber. Ammonia is not a known product of the discharge chamber, but due to the existence of nitrogen and hydrogen with ample energy to drive chemical reactions to completion it is possible that ammonia could be formed in the reaction chamber. The increased NO_x production could be explained by this reaction if ammonia produced in the discharge chamber was enhanced by the addition of humidity. The hydrogen radicals introduced by the decomposition of water vapor could react with the nitrogen radicals increasing the ammonia concentration past the equilibrium value. This would in turn, shift the equilibrium to the right, resulting in an increase in the NO_x concentration indicated by the Analyzer (more NO).

Another possible mechanism for increased NO_x production with the addition of humidity is:



If the production of NO₂⁻ is enhanced by the addition of water vapor to the chamber, the equilibrium could shift to the left resulting in an increase in N₂O₂⁻². High levels of N₂O₂⁻² in the chamber could possibly produce NO by the following reaction (45):



In the above reaction, N₂O₂⁻² from the previous proposed mechanism may be present over the equilibrium concentration, shifting the reaction to produce more NO.

In other words, nitric oxide has been formed from other oxides of nitrogen not previously detected by the NO_x analyzer.

The above reactions cited represent just a few of the possible mechanisms that could lead to the increased production of NO_x. Further research is definitely warranted to pinpoint the exact mechanism(s) that govern the NO_x production relationship with respect to humidity.

Possible Reasons for NO_x Decrease

Nitrogen has a triple bond, with an energy of 946 kJ, while water's bond energy is only 463 kJ. The water will absorb the corona power before the nitrogen because it requires less energy to break the bond, therefore it is more susceptible to decomposition. This theory is supported by Coffman (1), the oxygen or air fed into an ozonizer must be dry, if water vapor is present, the electrons and radicals will attack water molecules rather than the oxygen molecules, because corona attacks the most vulnerable species in the reaction chamber.

The above statements provide further insight into corona behavior. Assuming the corona attacks the most vulnerable molecule in the reaction chamber before attacking other more tightly bonded molecules, possibly at humidities above 35% and the optimized 60 volt setting, there wasn't enough energy left after attacking all water molecules to decompose an appreciable amount of N₂. If no nitrogen breakdown occurs then no oxides of nitrogen will result. At humidity levels below the 35% maximum, whatever mechanism that enhanced NO_x production had enough energy to proceed. Past the 35% maximum, the water vapor present in the chamber requires all the power available at the 60 volt setting, with no power left to decompose N₂ there would be no elemental nitrogen available to recombine to form NO_x, leading to the sharp decline in NO_x production.

These theories accurately supports the results of this research. Of course, further research needs to be done linking molecule vulnerability, power input, and byproduct formation in the ACPR. Figure 21 shows a crude graphical approximation of the points covered above.

Brief Note on Plasma Stability

Plasma stability at an optimized 60 volt setting was attained in approximately 8 minutes. Stability at optimized 40 and 50 volt settings didn't occur sometimes for 22 hours. This research shows most applications are enhanced by increased plasma power input. Lower primary voltages, as far as gaseous production goes, seem unnecessary to investigate further with any detail.

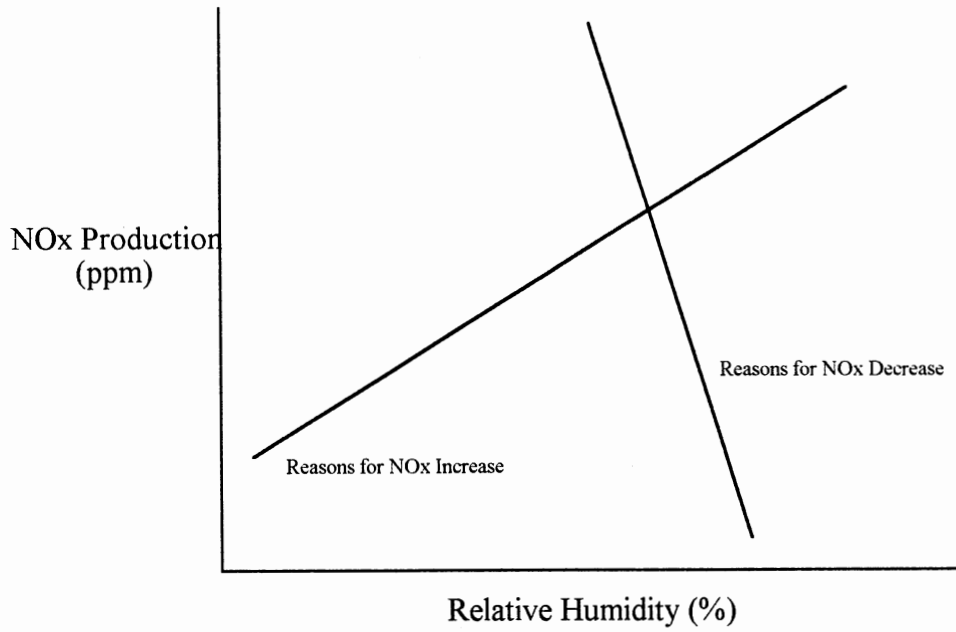


Figure 21. Representation of Possible NOx Production Mechanisms with Respect to Relative Humidity

CHAPTER VI

ADDITIONAL TESTING

Additional testing was undertaken to investigate the feasibility of using the ACPR as a destruction mechanism for NO_x, and to validate the proposed chemical reactions involving NO_x occurring in the discharge chamber. Destruction testing results will be presented first, followed by the chemical reaction validation. Destruction test data can be found in Appendix D.

Destruction Testing

Figure 22 shows the relationship between NO_x destruction and flow rate. All testing was conducted at an optimized 60 volt setting, using the 7459 ppm NO standard balanced in nitrogen. These tests were initialized to see if the plasma reactor is an effective method of destroying the oxides of nitrogen. Destruction efficiencies ranged from 66.48% to 99.33%. These tests proved the ACPR to be an efficient method of removing NO_x from a gas stream. Destruction efficiency decreases as flow rate increases. These results agree with findings from previous destruction studies (20, 36). Further investigation is necessary to examine ACPR destructive capabilities under approximate industrial process conditions to deduce true application possibilities.

Validation of Chemical Reaction Mechanisms

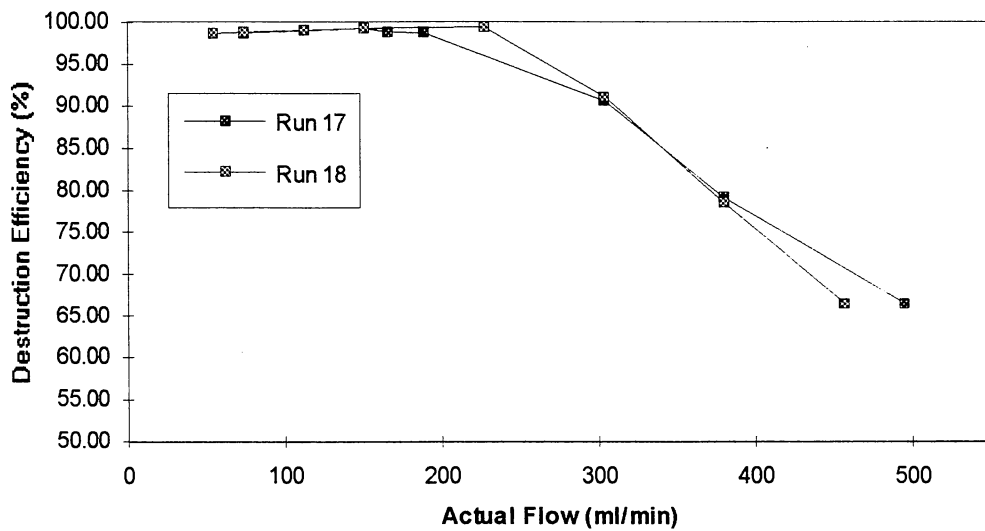


Figure 22. NO_x Destruction with Respect to Flow Rate Using A 7459 ppm Nitric Oxide, NO, Standard @ Optimized 60 volt Setting

The Thermal Electron NO_x Analyzer only detected NO and NO₂. With respect to the mechanisms presented in earlier sections, other oxides of nitrogen must be produced as precursors to the formation of NO and NO₂. This section of the research proves that there are other oxides of nitrogen being produced in the discharge chamber. The detection column used in the Ion Chromatograph only detected nitrate and nitrite in the samples analyzed. Further research is necessary to deduce the full range of nitrous oxides being produced in the plasma chamber. Condensate was collected over an extended period with the plasma operating variables fluctuating widely (i.e. primary voltage, flow rate, humidity). Bubbling of the post plasma gas through the NaOH solution was done at the maximum NO_x production level, 1700 ppm. Concentration test data calculated from graphical data from Figures 23, 24 & 25 can be found in Appendix F.

Through the use of a Dionex Series 2000i/SP Ion Chromatograph, both nitrate and nitrite were identified in the post plasma gas stream. Concentrations were deduced from a known standard curve previously prepared for the species in question. Condensate was collected in the cold trap and analyzed by the ion chromatograph, see Figure 23. The sample had to be diluted by 100,000 times to be accurately measured on the ion chromatograph. The peak at 3.48 represents nitrate concentration. See Appendix E for column response. The concentration of nitrate found in the sample was 623 g/l. These results when coupled with the pH approximation described in an earlier section, indicate the condensate was in fact extremely nitric acid. Sample concentration calculations can be found in Appendix A.

Figures 24 and 25 show the concentrations of nitrite and nitrate captured by the NaOH bubbler. Tests were performed at 35% relative humidity and the optimized 60 volt setting. The bubbled sample was diluted 100:1 prior to sample injection. In

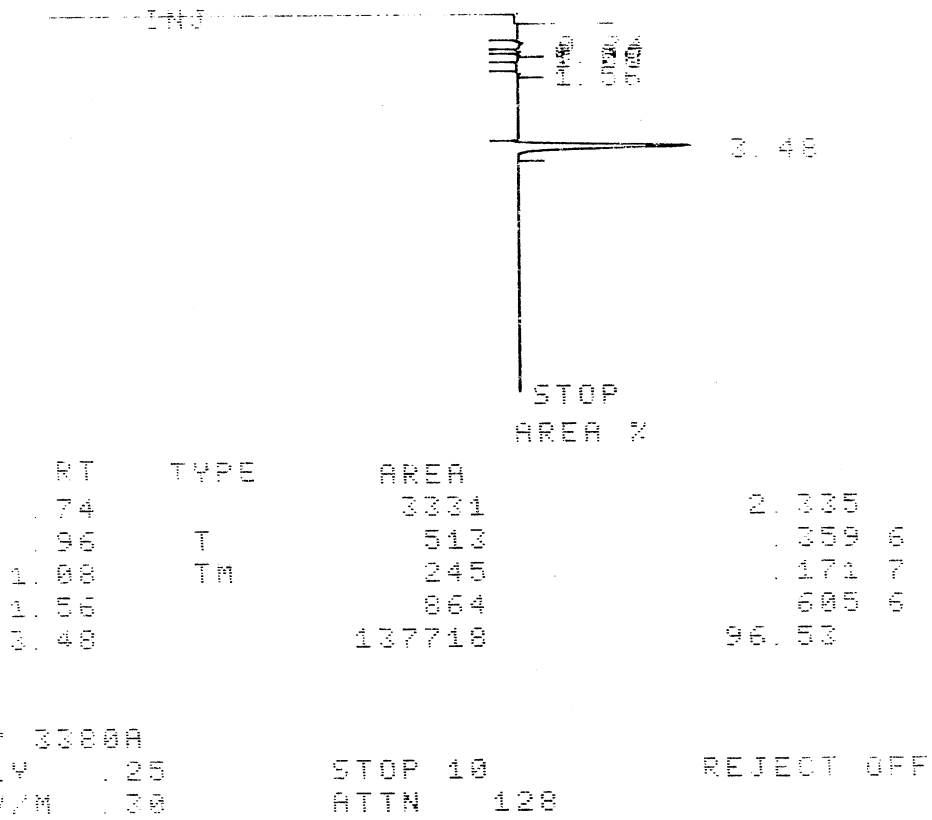


Figure 23. Graphical Representation of Nitrate Concentration in Condensate. 1:100,000 Dilution Nitrate Peak Occurs at 3.48 and has a Value of 137718, Indicated by the Dionex Ion Chromatograph

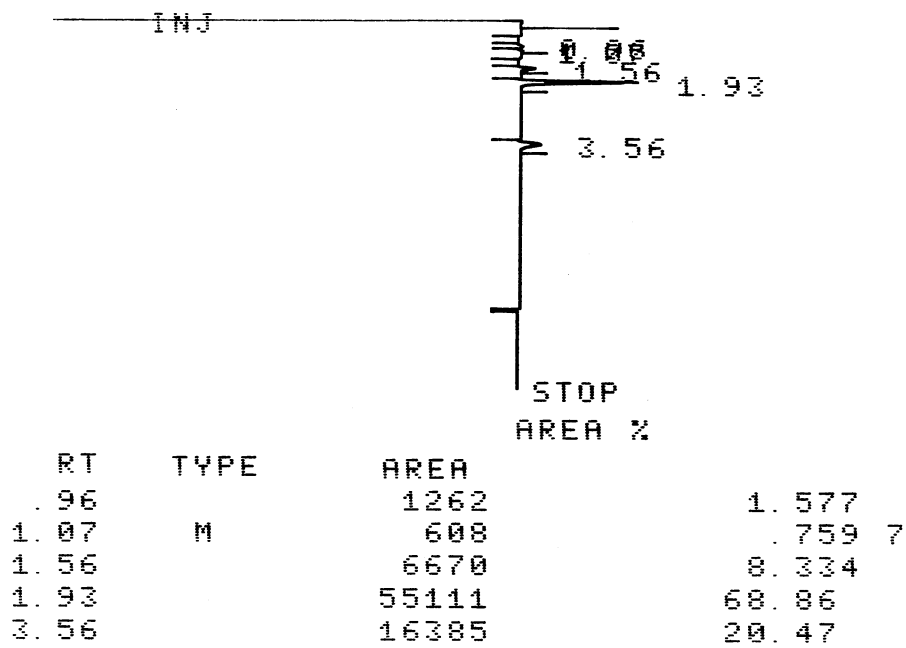


Figure 24. Graphical Representation of Nitrite & Nitrate Concentrations in the NaOH Solution. 1:100 Dilution. Nitrite Peak Occurs at 1.92 and has a Value of 55168, Nitrate Peak Occurs at 3.55 and has a Value of 16725 as Indicated by the Dionex Ion Chromatograph

Figure 24, the peak at 1.93 represents nitrite concentration and the peak at 3.56 represents nitrate concentration in the sample. The nitrite and nitrate concentrations were respectively 212 mg/l and 74 mg/l. From Figure 25 nitrite and nitrate concentrations are 212 mg/l and 76 mg/l. These tests were performed immediately after bubbling the gas through the NaOH solution for 5 hrs. These results provide minimal insight into the oxides of nitrogen produced in the discharge chamber. The only oxides of nitrogen detected by the Ion Chromatograph are nitrate and nitrite. The NO_x analyzer detects only NO and NO₂. These tests do not validate the reaction mechanisms proposed for increased NO_x production due to the introduction of water vapor into the reaction chamber, but do indicate that many different oxides of nitrogen may be produced in the discharge chamber. Further research is required to fully understand the spectrum of byproducts formed in the ACPR.

CHAPTER VII

CONCLUSIONS AND RECOMMENDATIONS

Research presented in this thesis was primarily directed towards proving the Alternating Current Plasma Reactor (ACPR), to be an effective method to produce the oxides of nitrogen, NO_x, at approximate atmospheric conditions. Production potential for NO_x was investigated with respect to electrical and gas flow plasma variables.

CONCLUSIONS

The conclusions from these experiments are as follows:

1. The ACPR has an optimum frequency at each primary voltage which yields a maximum power input to the reactor.
2. As primary voltage is increased, optimum conditions occur at progressively lower frequencies.
3. Humidity has little effect on overall plasma behavior at a given primary voltage (Reactor optimization shift is practically null).
4. NO_x production increases as primary voltage (power input) increases.
5. Maximum NO_x production using dry air occurs at the optimized condition for a specific primary voltage. On either side of the optimum frequency production drops off to negligible levels quickly.
6. As the flow rate is increased, the NO_x production decreases.
7. Humidity variation produced the most notable variation in NO_x production. A

steady increase in NO_x production occurs as the humidity rises from 10% to 35% relative humidity. After 35% the production rapidly decreases to background levels.

8. Maximum NO_x production occurred at high plasma power input, low flow rate, and 35% relative humidity.
9. The ACPR proved to be an effective method for the destruction of NO_x. Destruction efficiency was improved as the flow rate was decreased. Maximum efficiency for conversion was 99.33%.

RECOMMENDATIONS

1. Further research is necessary to determine the exact influence that humidity has on the production of the oxides of nitrogen. Testing needs to be done at various power levels and humidities to determine if the production peak is a function of water vapor in the discharge chamber, or if the peak production humidity can be influenced by power input to the reactor.
2. The full range of the oxides of nitrogen produced in the discharge chamber needs to be investigated.
3. Other production studies involving different gaseous reactants should be done. Very little has been done as far as monitoring gaseous products produced by the ACPR.
4. Diverse destruction studies need to be initiated. Examine how mixtures of airborne pollutants effect the destruction efficiency of a given substance.
5. Destruction studies more closely resembling industrial application possibilities need to be investigated to deduce industrial applicability.
6. Scale up of the reactor should be investigated. Can a cost effective plasma be generated with a large annular volume?

BIBLIOGRAPHY

- [1] Coffman, J. A., W. R. Browne, "Corona Chemistry." Scientific American Journal, 212(6), (1965): pp. 91 - 98.
- [2] Kanazawa, S., M. Kogoma, T. Moriwaki, and S. Ozazaki, "Stable glow plasma at atmospheric pressure." Journal of Applied Physics, 21 (1988): pp. 838 - 840.
- [3] Tevault, D. E., M. Chester, P. Simmons and J. Birmingham, "NO_x Production in a Silent Electric Discharge as a Function of Humidity, Frequency, and Power." Unpublished Results.
- [4] Lavoie, G. A., J. B. Heywood, and J. C. Keck, "Experimental and Theoretical Study of Nitric Oxide Formation in Internal Combustion Engines." Combustion Science and Technology, 1970: vol. 1, pp. 313 - 326
- [5] Weschler, C. J., "Indoor Ozone and Nitrogen Dioxide: A Potential Pathway to the Generation of Nitrate Radicals, Dinitrogen Pentaoxide, and Nitric Acid Indoors." Environmental Science and Technology, 1992: vol 26 No. 1, pp. 179 - 184
- [6] De Arellano, J. V., A. M. Talmon, and P. J. H. Builtjes, "A Chemically Reactive Plume Model for the NO-NO₂-NO₃ System." Atmospheric Environment 1990: vol 24A, No. 8, pp. 2237 - 2246
- [7] Brandvold, D. K., P. Martinez, and D. Dogruel, "Polarity Dependence of N₂O Formation From Corona Discharge." Atmospheric Environment , 1989: vol 23, No. 9, pp. 1881 - 1883
- [8] Chamberland, D. NASA Bioengineer, Verbal Communication regarding technical background on the necessity to produce NO_x. 1992.
- [9] Schwartzkopf, S.H., "Design of a Controlled Ecological Life Support System." Bioscience, 1992: vol 42, No. 7, pp. 526 - 534.
- [10] Chamberland, D., Knott, W. M., Sager, J. C., and R. Wheeler, "Controlled Ecological Life Support System (CLESS) Use of Plants for Human Life Support in Space." Florida Medical Journal, Sept. 1992.

- [11] Chamberland, D. W., "Advanced Life Support Systems in Lunar and Martian Environments Utilizing a Higher Plant Based Engineering Paradigm." International Conference for Environmental Systems, Seattle, July 1992.
- [12] Tsai, V. Y., "Conceptual Design and Performance Analysis of Frequency-Tuned Capacitive Discharge Reactors." PHD Discertation, Oklahoma State University, Stillwater (1990)
- [13] Piatt, M. A., "Methane Destruction in an Alternating Current Plasma Reactor." MS Thesis, Oklahoma State University, Stillwater (1988)
- [14] Mangrio, M. T., "Production of Titanium Dioxide Powder by the Oxidation of Titanium Tetrachloride in a Plasma Reactor." MS Thesis, Oklahoma State University, Stillwater (1992).
- [15] McEachron, K. B., "The Production of Nitric Oxides and Ozone by High Voltage Electric Discharges." Engineering Experiment Station, Bulletin No. 9, Purdue University, Lafayette, IN. 1922.
- [16] World Health Organization, Environmental Health Criteria: Oxides of Nitrogen, Chapter 1. United Nations Environment Programme, Geneva, 1977.
- [17] Lee, S. D., Nitrogen Oxides, Chapter 5. National Academy of Sciences, 1977.
- [18] Guicherit, R., D. van den Hout, "The NO_x Cycle", Air Pollution by Nitrogen Oxides, Elsevier Scientific Publishing Company, Amsterdam-Oxford-New York, 1982.
- [19] Posthumus, A. C., "Ecological Effects Associated With NO_x, Especially on Plants and Vegetation." Air Pollution by Nitrogen Oxides, Elsevier Scientific Publishing Company, Amsterdam-Oxford-New York, 1982.
- [20] Kremer, H., "Chemical and Physical Aspects of NO_x Formation." Air Pollution by Nitrogen Oxides, Elsevier Scientific Publishing Company, Amsterdam-Oxford-New York, 1982.
- [21] Cox, R. A., "Chemical Transformation Processes for NO_x Species in the Atmosphere." Air Pollution by Nitrogen Oxides, Elsevier Scientific Publishing Company, Amsterdam-Oxford-New York, 1982.
- [22] Balin, L. J., M. E. Sibert, L. A. Jonas and A. T. Bell. "Microwave Decomposition of Toxic Vapor Simulants." Environmental Science and Technology, 9(3), 254-258 (1975)

- [23] Loeb, L. B., "Fundamental Processes of Electrical Discharges in Gases." New York: John Wiley & Sons, Inc., 1939
- [24] Thornton, W. M., "The Electric Strength of Gases, Measured by Corona Discharge." Phil. Mag. 28, 666-678 (1939)
- [25] Calloway, D. H., "Basic data for planning life-support systems." Foundations of Space Biology and Medicine, vol. 3, 3-21. NASA, Washington, DC.
- [26] Hales, J. M., "The Role of NO_x as a Precursor of Acidic Deposition." Air Pollution by Nitrogen Oxides, Elsevier Scientific Publishing Company, Amsterdam-Oxford-New York, 1982.
- [27] Posthumus, A. C., "Ecological Effects Associated with NO_x, Especially on Plants and Vegetation." Air Pollution by Nitrogen Oxides, Elsevier Scientific Publishing Company, Amsterdam-Oxford-New York, 1982.
- [28] Hekstra, G. P., "Ecological and Biological Effects." Air Pollution by Nitrogen Oxides, Elsevier Scientific Publishing Company, Amsterdam-Oxford-New York, 1982.
- [29] Mansfield, T. A., Mary E. Whitmore and R. M. Law, "Effects of Nitrogen Oxides on Plants: Two Case Studies." Air Pollution by Nitrogen Oxides, Elsevier Scientific Publishing Company, Amsterdam-Oxford-New York, 1982.
- [30] VanDop, H., "Atmospheric Physical Processes." Air Pollution by Nitrogen Oxides, Elsevier Scientific Publishing Company, Amsterdam-Oxford-New York, 1982.
- [31] Gardner, D. E, F.J. Miller, J. W. Illing and J. A. Graham, "Non-Respiratory Function of the Lungs: Host Defenses Against Infection." Air Pollution by Nitrogen Oxides, Elsevier Scientific Publishing Company, Amsterdam-Oxford-New York, 1982.
- [32] Fraser, M. E., H. G. Eaton and R. S. Sheinson. "Initial Decomposition Mechanisms and Products of Dimethyl Methylphosphonate in an Alternating Current Discharge." Plasma Chemistry and Plasma Processing, 4(1), 1984.
- [33] Clothiaux, E. J., J. A. Koropchak and R. P. Moore. "Decomposition of an Organophosphorus Material in a Silent Discharge." Plasma Chemistry and Plasma Processing, 4(1), 1984.
- [34] Fraser, M. E. and R. S. Sheinson. "Electric Discharge Induced Oxidation of Hydrogen Cyanide." Plasma Chemistry and Plasma Processing, 4(1), 1984.

- [35] Neely, W. C., S. R. Best and E. J. Clothiaux. "The Decomposition of Gas Phase Formaldehyde by Plasma Discharge." In Proceedings of the 1984 Scientific Conference on Chemical Defense Research, Aberdeen, Maryland (1984).
- [36] Desai, V. R., "Decomposing of Hydrogen Sulfide in an Alternating Current, Frequency Tuned Plasma Reactor." MS Thesis, Oklahoma State University, Stillwater (1992).
- [37] Sawyer, C. N. and P. L. McCarty, Chemistry for Environmental Engineering, McGraw Hill, New York, (1978).
- [38] World Health Organization, Environmental Health Criteria, Oxides of Nitrogen. World Health Organization, United Kingdom, 1977
- [39] Dibelius, N. R., J. C. Fraser, M. Kawahata and C. D. Doyle. "Corona Processing of Coal." Chem. Eng. Prog. 60(6), 1964, 41 - 44.
- [40] Moore, R. R., and J. G. Birmingham, "The Decomposition of Toxic Chemicals in a Low Temperature Plasma Device." HAZPRO 1987 Conference Proceedings, Chattanooga, Tennessee (June 8 - 12, 1987).
- [41] Davis, S. R. and D. E. Tevault, "FTIR Studies of Plasma-Induced Decomposition of Dimethylsulfide in an Air-like Environment." HAZPRO 1987 Conference Proceedings, Chattanooga, Tennessee (June 8 - 12, 1987).
- [42] Bedell, F., The Principles of the Transformer. New York: Macmillan Company; 1986.
- [43] Veenstra, J. N., (Oklahoma State University). Personal Communication.
- [44] Johannes, A. J., (Oklahoma State University). Personal Communication.
- [45] Moeller, T., Inorganic Chemistry, New York: John Wiley & Sons, Inc, 1952

APPENDIX A

SAMPLE CALCULATIONS

Calculation of Concentration from Ion Chromatograph Output

$$\text{Nitrate Concentration (mg/l)} = \frac{\text{PeakArea}}{(22.1)(1000)} (\text{Dilution})$$

$$\text{Nitrite Concentration (mg/l)} = \frac{\text{PeakArea}}{(26)(1000)} (\text{Dilution})$$

Sample Calculation from Figure 24.

Nitrate Peak Area = 16385

Corresponding to a concentration of 74 mg/l

Nitrite Peak Area = 55111

Corresponding to a concentration of 212 mg/l

Sample Destruction Efficiency Calculation

Destruction Efficiency (%) = (NO Standard Concentration - ppm Remaining)/NO Standard

Sample Calculation from Figure 22, Run 17

NO Standard (ppm) = 7459 ppm
Remaining Concentration = 50 ppm

$$\begin{aligned} \% \text{ Destruction} &= ((7459 - 50)/7459)(100) \\ &= 99.33 \% \end{aligned}$$

APPENDIX B

REACTOR OPTIMIZATION TEST DATA

TABLE 7

REACTOR OPTIMIZATION TEST DATA CORRESPONDING TO FIGURE 14
RUN 1

Primary Voltage: 20 V

Type of Gas: Dry Air

Flow Rate: 118 ml/min

Frequency - Hz	Secondary Voltage - kV	Frequency - Hz	Secondary Voltage - kV
300	2.80	820	11.96
400	3.20	830	11.96
500	3.64	840	11.64
550	4.04	850	11.58
600	4.80	860	11.20
650	5.50	870	10.60
700	6.80	900	9.68
750	9.20	950	7.58
760	9.66	1000	5.26
770	10.40	1100	3.60
780	10.80	1200	2.60
790	11.24	1300	2.00
800	11.62	1400	1.60
810	11.80	1500	0.80

TABLE 8

REACTOR OPTIMIZATION TEST DATA CORRESPONDING TO FIGURE 14
RUN 2

Primary Voltage: 30 V

Type of Gas: Dry Air

Flow Rate: 118 ml/min

Frequency - Hz	Secondary Voltage - kV	Frequency - Hz	Secondary Voltage - kV
300	4.40	790	14.00
400	4.80	800	14.00
500	5.60	810	13.80
550	6.38	820	13.68
600	7.24	830	13.60
650	8.76	840	13.40
700	11.00	850	13.20

TABLE 8 (CONTINUED)

Frequency - Hz	Secondary Voltage - kV	Frequency - Hz	Secondary Voltage - kV
710	11.60	900	13.20
720	12.36	950	9.80
730	12.74	1000	7.56
740	13.20	1100	5.16
750	13.60	1200	3.80
760	13.80	1300	2.80
770	13.98	1400	2.20
780	14.00	1500	1.80

TABLE 9

REACTOR OPTIMIZATION TEST DATA CORRESPONDING TO FIGURE 14
RUN 3

Primary Voltage: 40 V

Type of Gas: Dry Air

Flow Rate: 118 ml/min

Frequency - Hz	Secondary Voltage - kV	Frequency - Hz	Secondary Voltage - kV
300	6.00	730	15.60
400	6.60	740	15.20
450	7.20	750	15.18
500	7.84	760	14.84
550	8.80	780	14.76
600	10.00	800	14.40
650	12.30	850	13.60
660	12.86	900	12.60
670	13.64	1000	9.28
680	14.36	1100	6.60
690	14.80	1200	4.80
700	15.20	1300	3.80
710	15.40	1400	2.84
720	15.50	1500	2.40

TABLE 10

REACTOR OPTIMIZATION TEST DATA CORRESPONDING TO FIGURE 14
RUN 4

Primary Voltage: 50 V

Type of Gas: Dry Air

Flow Rate: 118 ml/min

Frequency - Hz	Secondary Voltage - kV	Frequency - Hz	Secondary Voltage - kV
300	7.56	680	16.32
400	8.40	690	16.00
500	9.92	700	15.96
550	11.20	710	15.80
560	11.60	720	15.60
570	11.98	750	15.40
580	12.44	800	14.80
590	13.00	850	14.00
600	13.66	900	13.20
610	14.40	950	13.00
620	15.16	1000	10.60
630	15.60	1100	8.00
640	16.00	1200	6.00
650	16.20	1300	4.60
660	16.20	1400	3.60
670	16.20	1500	3.00

TABLE 11

REACTOR OPTIMIZATION TEST DATA CORRESPONDING TO FIGURE S 14 & 15
RUN 5

Primary Voltage: 60 V

Type of Gas: Dry Air

Flow Rate: 118 ml/min

Frequency - Hz	Secondary Voltage - kV	Frequency - Hz	Secondary Voltage - kV
300	9.16	630	16.68
400	10.16	640	16.56
450	10.88	650	16.40
500	12.40	660	16.20
520	13.00	700	15.80
530	13.60	750	15.24

TABLE 11 (CONTINUED)

Frequency - Hz	Secondary Voltage - kV	Frequency - Hz	Secondary Voltage - kV
540	14.04	800	14.60
550	14.86	850	14.00
560	15.60	900	13.20
570	16.36	1000	10.84
580	16.74	1100	8.00
590	16.80	1200	7.20
600	17.00	1300	5.40
610	16.80	1400	4.40
620	16.80	1500	3.60

TABLE 12

REACTOR OPTIMIZATION TEST DATA CORRESPONDING TO FIGURE 16
RUN 6

Primary Voltage: 60 V

Type of Gas: Dry Air

Type of Gas: Air 45% Relative Humidity

Flow Rate: 118 ml/min

Frequency - Hz	Secondary Voltage - kV	Frequency - Hz	Secondary Voltage - kV
300	9.16	300	9.20
400	10.16	400	10.40
500	12.40	500	12.60
550	14.86	550	14.80
600	17.00	600	16.80
650	16.40	650	17.60
700	15.80	700	16.80
800	14.60	800	15.20
900	13.20	900	12.80
1000	10.84	1000	11.20
1100	8.00	1100	9.60
1200	7.20	1200	7.60
1300	5.40	1300	5.60
1400	4.40	1400	4.40
1500	3.60	1500	3.60

APPENDIX C

NO_x PRODUCTION TEST DATA

TABLE 13

NO_x PRODUCTION VS. PRIMARY VOLTAGE TEST DATA CORRESPONDING TO FIGURE 17
RUNS 7, 8 & 9

Tests Conducted at Optimized Settings

Type of Gas: Dry Air

Flow Rate: 118 ml/min

Primary Voltage (V)	NO _x (ppm) Run 7	NO _x (ppm) Run 8	NO _x (ppm) Run 9
20	11	28	30
30	145	100	125
40	170	180	240
50	220	260	240
60	630	640	800

TABLE 14

NO_x PRODUCTION VS. FREQUENCY TEST DATA CORRESPONDING TO FIGURE 18
RUNS 10 & 11

Frequency Variation at Various Primary Voltages

Type of Gas: Dry Air

Flow Rate: 118 ml/min

Run #10 Frequency (Hz)	Run #10 NO _x (ppm)	Run #11 Frequency (Hz)	Run #11 NO _x (ppm)
400	50	350	2
530	980	425	4
650	920	500	880
750	840	530	925
900	26	560	950
		590	880
		650	15
		700	11

TABLE 15

NO_x PRODUCTION VS. FLOW RATE TEST DATA CORRESPONDING TO FIGURE 19
 RUNS 12, 13 & 14

Flow Variation at Primary Voltage of 60 volts and Optimized Conditions

Type of Gas: Dry Air

Flow Rate: 118 ml/min

Flow Rate (ml/min)	Run #12 NO _x (ppm)	Run #13 NO _x (ppm)	Run #14 NO _x (ppm)
69		720	710
107	640	640	
122			580
136	580	560	
152		540	
168	515	520	
199	480		470
226	445		
275			410
306	415	490	
382			
497			

TABLE 16

NO_x PRODUCTION VS RELATIVE HUMIDITY TEST DATA CORRESPONDING TO FIGURE 20
 RUNS 15 & 16

Humidity Variation at Primary Voltage of 60 volts and Optimized Conditions

Type of Gas: Humified Air

Flow Rate: 146 ml/min

Humidity (%)	Run #15 NO _x (ppm)	Run #16 NO _x (ppm)
10	540	540
25	840	1050
30	1450	1600
35	1650	1700
40	1200	

TABLE 16 (CONTINUED)

Humidity (%)	Run #15 NOx (ppm)	Run #16 NOx (ppm)
45	10	130
55	6	
65	3	7

APPENDIX D

NO_x DESTRUCTION TEST DATA

TABLE 17

NO_x DESTRUCTION VS. FLOW RATE TEST DATA CORRESPONDING TO FIGURE 22
RUN 17

Tests Conducted Optimized 60 Volt Setting

Type of Gas: 7459 NO Standard Balanced in Nitrogen

Flow Rate: Varied

Flow (ml/min)	Θ	Remaining Concentration (ppm)	Destruction Efficiency (%)
100	45	95	98.73
200	22.5	50	99.33
220	20.5	85	98.86
250	18	90	98.79
400	11.3	700	90.62
500	9	1550	79.22
650	6.9	2500	66.48

TABLE 18

NO_x DESTRUCTION VS. FLOW RATE TEST DATA CORRESPONDING TO FIGURE 22
RUN 18

Tests Conducted Optimized 60 Volt Setting

Type of Gas: 7459 NO Standard Balanced in Nitrogen

Flow Rate: Varied

Flow (ml/min)	Remaining Concentration (ppm)	Destruction Efficiency (%)
75	100	98.66
100	85	98.86
150	70	99.06
200	50	99.88
300	40	99.46
400	660	91.15
500	1600	78.55
600	2500	66.48

APPENDIX E

ION CHROMATOGRAPH COLUMN RESPONSE



**IONPAC AS4A-SC 4mm (10-32) ANALYTICAL COLUMN (P/N 043174)
TEST CHROMATOGRAM**

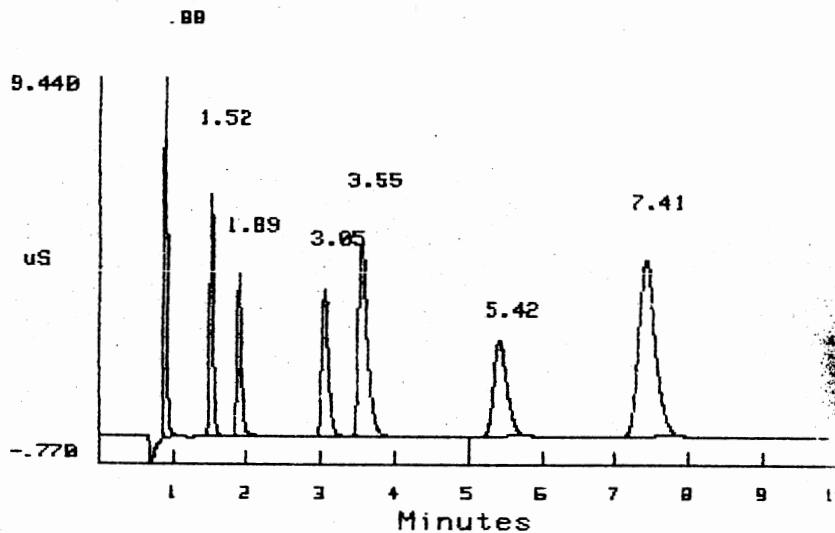
This chromatogram was obtained during a quality control test. Please note that test fixtures were used, so slight variations from the test chromatogram may occur on your instrument. Eluent batch and laboratory climate can also affect chromatographic performance.

Eluent: 1.8 mM Na₂CO₃/1.7 mM NaHCO₃

Flow Rate: 2.0 mL/min

Detection: Suppressed Conductivity at 30 μ SFS

Standard: 25 μ L of:	1. Fluoride	2.0 mg/L	5. Nitrate	10.0 mg/L
	2. Chloride	3.0 mg/L	6. Phosphate	15.0 mg/L
	3. Nitrite	5.0 mg/L	7. Sulfate	15.0 mg/L
	4. Bromide	10.0 mg/L		



APPENDIX F

NITRITE AND NITRATE CONCENTRATIONS DEDUCED
FROM ION CHROMATOGRAPH TESTING

TABLE 19

CONCENTRATION DATA FROM VARIOUS SAMPLES USING THE ION
CHROMATOGRAPH CORRESPONDING TO FIGURES 23, 24, & 25

Tests Conducted Optimized 60 Volt Setting

Type of Gas: 35% Relative Humidity Breathing Air

Testing Apparatus: Dionex Series 2000i/SP Ion Chromatograph
w/ a Ionpac AS4A-SC 4mm Analytical Column

Sample	Nitrate (mg/l)		Nitrite (mg/l)	
Condensate	623,000		--	
NaOH Solution	Trial #1 212	Trial #2 212	Trial #1 74	Trial #2 76

2
VITA

Scott B. Robinowitz

Candidate for the Degree of

Master of Science

Thesis: PRODUCTION OF NO_x IN AN ALTERNATING CURRENT PLASMA REACTOR

Major Field: Environmental Engineering

Biographical:

Personal Data: Born in Tulsa, Oklahoma, January 9, 1969.

Education: Graduated from Washington High School, Tulsa, Oklahoma, in May 1987; received Bachelor of Science Degree in Mechanical Engineering from Tulane University in New Orleans, Louisiana May, 1991; completed requirements for the Master of Science degree at Oklahoma State University in December, 1992.

Professional Experience:

Intern Engineer, Grand Resources, Tulsa, Ok; Field Engineer, Reservoir Engineer